spots of normal pulp tissue compared with periodontal ligament (Supplementary Fig. S1D–F).

There have been no specific markers for pulp. Thus, some specific markers for periodontal ligament were used to further confirm normal pulp regeneration. Expression of

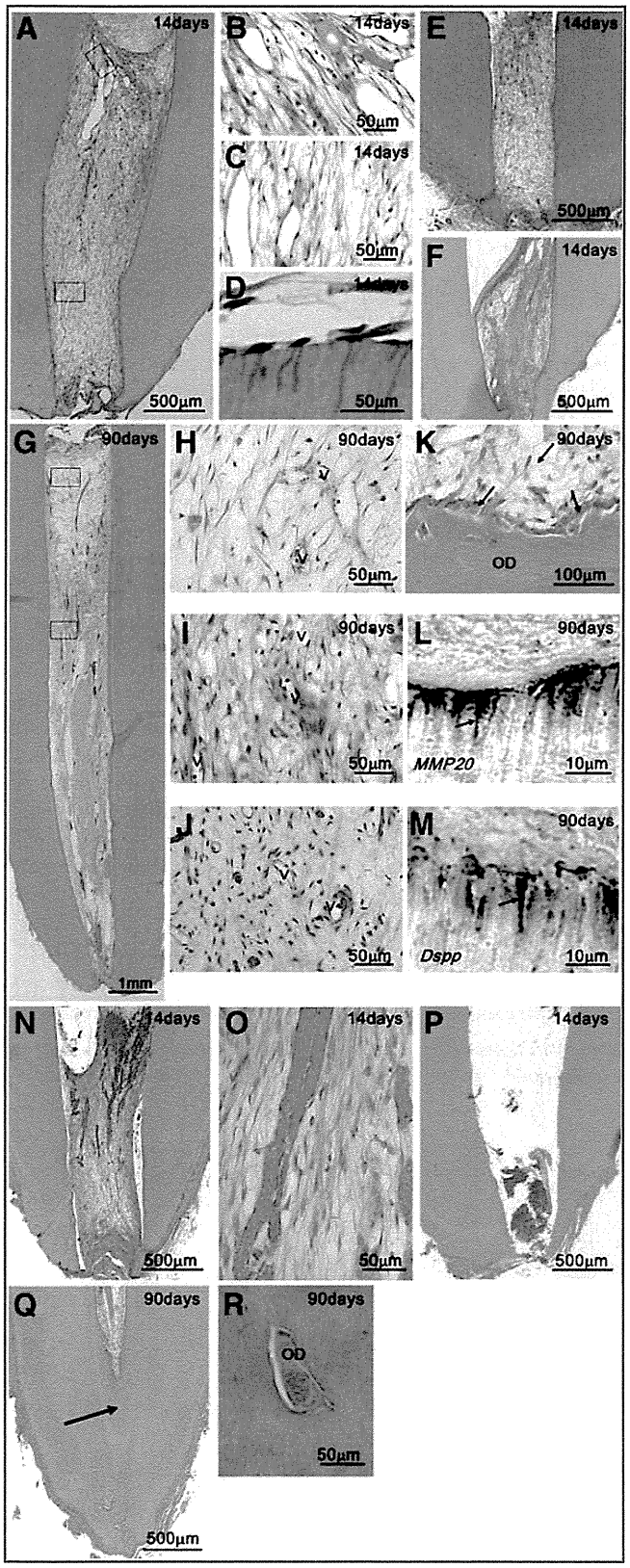

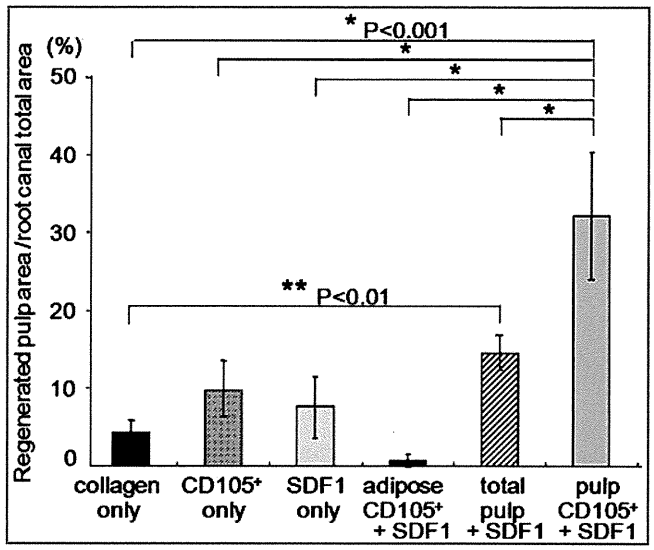

FIG. 6. Ratio of regenerated area to root canal area on day 14. Data are expressed as means ± standard deviation of five determinations. Statistical analysis was performed by the nonpaired Student's *t*-test.

axin2,[13] *periostin*,[14] and asporin/ *PLAP-1*[15] mRNA was much higher (25,531-fold, 179-fold, and 11-fold) in normal periodontal ligament than that in the regenerated tissue on day 28, respectively. Those genes were similarly expressed in a very low level in normal pulp compared with the regenerated tissue (0.4-fold, 0.4-fold, and 2.4-fold, respectively) (Fig. 8A). *Collagen αI(I)* was 9.3 times more expressed in periodontal ligament compared with the regenerated tissue, although this expression was not different between normal pulp and the regenerated tissue (Fig. 8A). *Syndecan3* and *TenascinC*, known to be highly expressed in pulp,[16,17] were 14.3 times and 50.0 times more expressed in the regenerated tissue compared with periodontal ligament, although those expressions in the regenerated tissue were similar to those in normal pulp (Fig. 8B). Hierachical clustering based on Affymetrix data produced a clear pattern separation of normal pulp tissue and the regenerated tissue from periodontal ligament (Supplementary Fig. S1G). Thus, the two-dimensional

FIG. 5. Complete regeneration of pulp tissue after autologous transplantation of $CD105^+$ cells with SDF-1 in the emptied root canal after pulpectomy in dogs. **(A–F)** Fourteen days after transplantation. **(A–D)** Pulp $CD105^+$ cells with SDF-1. **(E)** Pulp $CD105^+$ cells only. **(F)** SDF-1 only. **(G–I, K–M)** Ninety days after transplantation of pulp $CD105^+$ cells with SDF-1. **(H, I)** Newly formed blood vessels (v) in the upper part and the middle part of regenerated tissue. **(J)** Normal pulp tissue. **(K)** Odontoblastic cells (arrows) lining to newly formed osteodentin/tubular dentin (OD) along with the dentinal wall. **(L, M)** *In situ* hybridization analyses of odontoblast differentiation (arrows). **(L)** Enamelysin/matrix metalloproteinase 20 (MMP-20). **(M)** Dentin sialophosphoprotein (Dspp). **(N–P)** Fourteen days after transplantation. **(N, O)** Total pulp cells with SDF-1. **(P)** Adipose-derived $CD105^+$ cells with SDF-1. **(Q, R)** Ninety days after transplantation of total pulp cells with SDF-1. Mineralized tissue (arrow) and osteodentin (OD). Color images available online at www.liebertonline.com/tea

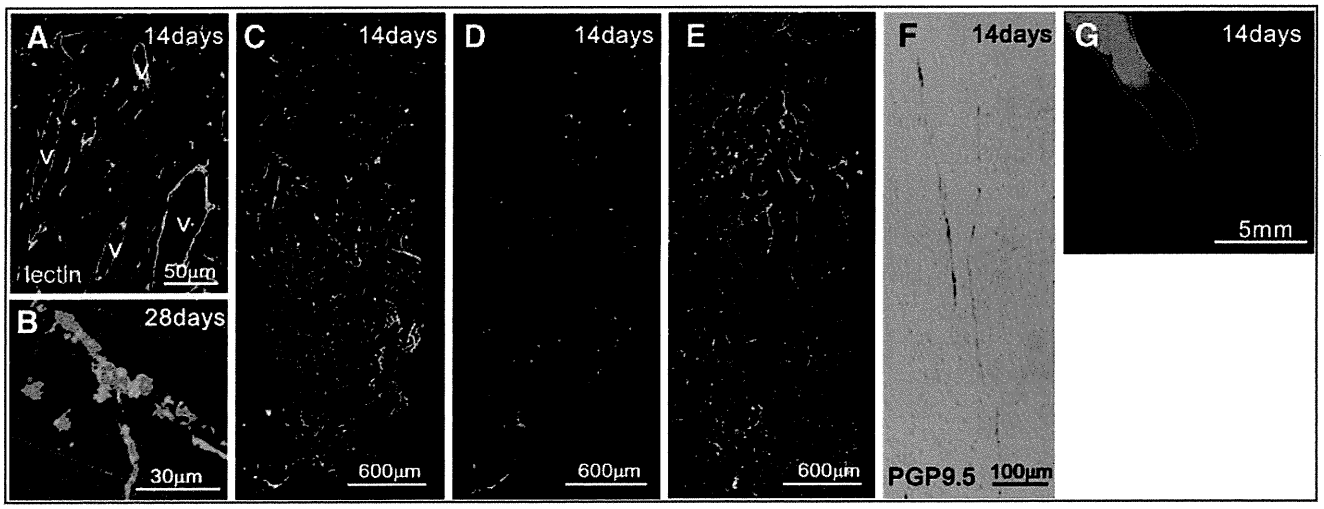

FIG. 7. **(A)** Immunostaining with BS-1 lectin. v: newly formed capillaries. **(B–E)** Three-dimensional images of new vascularization by whole mount immunostaining with lectin. **(B)** Note transplanted CD105$^+$ cells in the vicinity of the newly formed capillaries. **(D)** The DiI labeled transplanted cells located overall in the tissue. **(E)** Normal pulp tissue. **(F)** Immunostaining with PGP 9.5. **(G)** Neurogenesis in newly formed pulp tissue (white dotted line) connecting to inferior alveolar nerve. Color images available online at www.liebertonline.com/tea

electrophoretic analyses and the gene expression analyses suggested that the regenerated pulp tissue was identical to true functional normal pulp.

Discussion

Regeneration of pulp tissue is an unmet need in endodontic therapy. The critical requirements for pulp regeneration are morphogenesis of pulp tissue replete with angiogenesis/vasculogenesis and neurogenesis.[3,18] The induction of pulp-like tissue has been reported in a tooth slice model of subcutaneous transplantation in immunodeficient mice, by filling of pulp stem cells and dentin matrix protein 1 (DMP1) together[19] or stem cells from exfoliated deciduous teeth only[20] in a thin tooth slice. Similarly, another model for the induction of pulp-like tissue was subcutaneous transplantation of human tooth root fragment (6–7 mm long) with an enlarged root canal (1.0–1.25 mm in diameter) with one end sealed with mineral trioxide aggregate cement. Stem/progenitor cells from apical papilla and dental stem cells were inserted into the root. Pulp-like tissue with well-established vascularity and a continuous layer of odontoblast-like cells along the dentinal wall were observed as demonstrating the feasibility of pulp regeneration.[21] The novel finding in this investigation was the complete regeneration of whole pulp tissue after pulpectomy without tooth extraction by autologous pulp CD105$^+$ cell transplantation with SDF-1 in mature teeth with complete apical closure.

Human pulp CD105$^+$ cells have demonstrated angiogenesis/vasculogenic and neurogenic potential.[8] The SDF-1-CXCR4 axis plays a role in stem cell homing even in adulthood, especially after ischemia.[22] In this investigation, *CXCR4* was highly expressed in canine pulp CD105$^+$ cells. The regenerated pulp-like tissue was more in pulp CD105$^+$

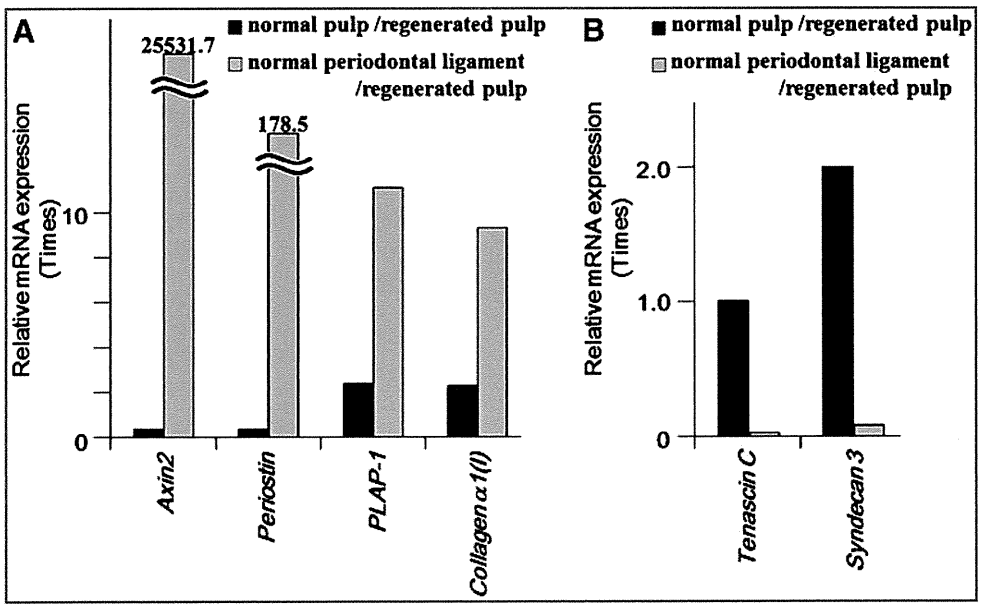

FIG. 8. Relative mRNA expression of cytokines of markers for periodontal ligament **(A)**, and for pulp **(B)** by real-time reverse transcription-polymerase chain reaction in regenerated pulp, normal pulp, and adipose periodontal tissue. The experiments were repeated four times, and one represented experiment is presented.

cells with SDF-1 compared with CD105$^+$ cells alone or SDF-1 alone. Therefore, these results suggested the combinatory effect of SDF-1 and pulp CD105$^+$ cells, especially SDF-1-CXCR4 axis for whole pulp regeneration. Similar contributions of SDF-1-CXCR4 axis, the 'homing' of stem cells expressing CXCR4 to a hypoxic-ischemic lesion where expression of SDF-1 significantly increased, have been reported in the rat ischemic brain after transplantation of human umbilical cord blood cells,[23] and in the myocardial ischemia,[24] or a subfraction of side population cells.[25]

Pulp tissue is readily available from discarded permanent teeth such as third molar and deciduous teeth after extraction. The autologous pulp stem cell source, however, is limited to patients who have discarded teeth with adequate pulp. Higher ratio of CD73 and CD150 positive cells and higher expression of *CXCR4*, *Sox2*, and *Bmi1* mRNA is observed in pulp CD105$^+$ cells compared with adipose CD105$^+$ cells, suggesting more stemness of pulp CD105$^+$ cells. Higher angiogenic and neurogenic potential and higher expression of a variety of proangiogenic factors and neurotrophic factors in pulp CD105$^+$ cells is compared with adipose CD105$^+$ cells *in vitro*, and expression of cytokines *VEGF-A* and *GM-CSF* mRNA by the transplanted pulp stem cells in the vicinity of the newly formed vasculature in the regenerated pulp,[26] implying that the higher trophic actions of pulp CD105$^+$ cells on endothelial cells promote neovascularization. Thus, pulp CD105$^+$ cells are a more useful cell source in induction of pulp regeneration by cell therapy compared with adipose CD105$^+$ cells and total pulp cells.

The routine translation of the current findings to the clinic is dependent on the use of autologous pulp in normal healthy patients. However, in the aged and in patients with diabetes, the pulp tissue may be limiting and may require novel approaches.

Conclusion

Our data demonstrate for the first time that pulp CD105$^+$ cells with SDF-1 induce complete pulp regeneration replete with neurogenesis and vasculogenesis *in vivo* in the adult dog after experimental pulpectomy. This cell therapy demonstrates the potential clinical utility of fractionated CD105$^+$ cells for endodontic treatment for conservation of teeth in dentistry.

Acknowledgments

This work was supported by grants of Collaborative Development of Innovative Seeds, potentiality verification stage from Japan Science and Technology Agency, a Grant-in-Aid for Scientific Research from the Ministry of Education, and the Research Grant for Longevity Sciences (21A-7) from the Ministry of Health, Labour, and Welfare (M.N.), Science, Sports, and Culture, Japan, #20390504 (M.N.), #21791872 (K.I.).

Disclosure Statement

The authors indicate no potential conflicts of interest.

References

1. Nakashima, M., and Akamine, A. The application of tissue engineering to regeneration of pulp and dentin in endodontics. J Endod **31,** 711, 2005.
2. Nakashima, M., and Reddi, A.H. The application of bone morphogenetic proteins to dental tissue engineering. Nature Biotech **21,** 1025, 2003.
3. Hargreaves, K.M., Giesler, T., Henry, M., and Wang, Y. Regeneration potential of the young permanent tooth: what does the future hold? J Endod **34,** S51, 2008.
4. Huang, G.T. Apexification: the beginning of its end. Int Endod J **42,** 855, 2009.
5. Barry, F.P., Boynton, R.E., Haynesworth, S., Murphy, J.M., and Zaia, J. The monoclonal antibody SH-2, raised against human mesenchymal stem cells, recognizes an epitope on endoglin (CD105). Biochem Biophys Res Commun **265,** 134, 1999.
6. Wynn, R.F., Hart, C.A., Corradi-Perini, C., O'Neill, L., Evans, C.A., Wraith, J.E., Fairbairn, L.J., and Bellantuono, I. A small proportion of mesenchymal stem cells strongly expresses functionally active CXCR4 receptor capable of promoting migration to bone marrow. Blood **104,** 2643, 2004.
7. Dar, A., Goichberg, P., Shinder, V., Kalinkovich, A., Kollet, O., Netzer, N., Margalit, R., Zsak, M., Nagler, A., Hardan, I., Resnick, I., Rot, A., and Lapidot, T. Chemokine receptor CXCR4-dependent internalization and resecretion of functional chemokine SDF-1 by bone marrow endothelial and stromal cells. Nat Immunol **6,** 1038, 2005.
8. Nakashima, M., Iohara, K., and Sugiyama, M. Human dental pulp stem cells with highly angiogenic and neurogenic potential for possible use in pulp regeneration. Cytokine Growth Factor Rev **20,** 435, 2009.
9. Lima e Silva, R., Shen, J., Hackett, S.F., Kachi, S., Akiyama, H., Kiuchi, K., Yokoi, K., Hatara, M.C., Lauer, T., Aslam, S., Gong, Y.Y., Xiao, W.H., Khu, N.H., Thut, C., and Campochiaro, P.A. The SDF-1/CXCR4 ligand/receptor pair is an important contributor to several types of ocular neovascularization. FASEB J **21,** 3219, 2007.
10. van Weel, V., Seghers, L., de Vries, M.R., Kuiper, E.J., Schlingemann, R.O., Bajema, I.M., Lindeman, J.H., Delis-van Diemen, P.M., van Hinsbergh, V.W., van Bockel, JH., and Quax, P.H. Expression of vascular endothelial growth factor, stromal cell-derived factor-1, and CXCR4 in human limb muscle with acute and chronic ischemia. Arterioscler Thromb Vasc Biol **27,** 1426, 2007.
11. Iohara, K., Zheng, L., Ito, M., Tomokiyo, A., Matsushita, K., and Nakashima, M. Side population cells isolated from porcine dental pulp tissue with self-renewal and multipotency for dentinogenesis, chondrogenesis, adipogenesis, and neurogenesis. Stem Cells **24,** 2493, 2006.
12. Iohara, K., Zheng, L., Wake, H., Ito, M., Nabekura, J., Wakita, H., Nakamura, H., Into, T., Matsushita, K., and Nakashima, M. A novel stem cell source for vasculogenesis in ischemia: subfraction of side population cells from dental pulp. Stem Cells **26,** 2408, 2008.
13. Lohi, M., Tucker, A.S., and Sharpe, P.T. Expression of Axin2 indicates a role for canonical Wnt signaling in development of the crown and root during pre- and postnatal tooth development. Dev Dyn **239,** 160, 2010.
14. Suzuki, H., Amizuka, N., Kii, I., Kawano, Y., Nozawa-Inoue, K., Suzuki, A., Yoshie, H., Kudo, A., and Maeda, T. Immunohistochemical localization of periostin in tooth and its surrounding tissues in mouse mandibles during development. Anat Rec Part A **281,** 1264, 2004.
15. Nakamura, S., Terashima, T., Yoshida, T., Iseki, S., Takano, Y., Ishikawa, I., and Shinomura, T. Identification of genes preferentially expressed in periodontal ligament: specific

expression of a novel secreted protein, FDC-SP. Biochem Biophys Res Commun **338,** 1197, 2005.
16. Hikake, T., Mori, T., Iseki, K., Hagino, S., Zhang, Y., Takagi, H., and Yokoya, S., Wanaka, A. Comparison of expression patterns between CREB family transcription factor OASIS and proteoglycan core protein genes during murine tooth development. Anat Embyol (Berl) **206,** 373, 2003.
17. Zhang, X., Schuppan, D., Becker, J., Reichart, P., and Gelderblom, H.R. Distribution of undulin, tenascin, and fibronectin in the human periodontal ligament and cementum: comparative immunoelectron microscopy with ultra-thin cryosections. J Histochem Cytochem **41,** 245, 1993.
18. Murray, PE, Garcia-Godoy, F., and Hargreaves, K.M. Regenerative endodontics: a review of current status and a call for action. J Endod **33,** 377, 2007.
19. Prescott, R.S., Alsanea, R., Fayad, M.I., Johnson, B.R., Wenckus, C.S., Hao, J., John, A.S., and George, A. *In vivo* generation of dental pulp-like tissue by using dental pulp stem cells, a collagen scaffold, and dentin matrix protein 1 after subcutaneous transplantation in mice. J Endod **34,** 421, 2008.
20. Cordeiro, M.M., Dong, Z., Kaneko, T., Zhang, Z., Miyazawa, M., Shi, S., Smith, A.J., and Nör, J.E. Dental pulp tissue engineering with stem cells from exfoliated deciduous teeth. J Endod **34,** 962, 2008.
21. Huang, G.T., Yamaza, T., Shea, L.D., Djouad, F., Kuhn, N.Z., Tuan, R.S., and Shi, S. Stem/progenitor cell-mediated *de novo* regeneration of dental pulp with newly deposited continuous layer of dentin in an *in vivo* model. Tissue Eng Part A **16,** 605, 2010.
22. Zaruba, M.M., and Franz, W.M. Role of the SDF-1-CXCR4 axis in stem cell-based therapies for ischemic cardiomyopathy. Expert Opin Biol Ther **10,** 321, 2010.
23. Rosenkranz, K., Kumbruch, S., Lebermann, K., Marschner, K., Jensen, A., Dermietzel, R., and Meier, C. The chemokine SDF-1/CXCL12 contributes to the 'homing' of umbilical cord blood cells to a hypoxic-ischemic lesion in the rat brain. J Neurosci Res **88,** 1223, 2010.
24. Wang, Y., Haider, H.Kh., Ahmad, N., Zhang, D., and Ashraf, M. Evidence for ischemia induced host-derived bone marrow cell mobilization into cardiac allografts. J Mol Cell Cardiol **41,** 478, 2006.
25. Liang, S.X., Tan, T.Y., Gaudry, L., and Chong, B. Differentiation and migration of Sca1+/CD31- cardiac side population cells in a murine myocardial ischemic model. Int J Cardiol **138,** 40, 2010.
26. Iohara, K., Zheng, L., Ito, M., Ishizaka, R., Nakamura, H., Into, T., Matsushita, K., and Nakashima, M. Regeneration of dental pulp after pulpotomy by transplantation of CD31(-)/CD146(-) side population cells from a canine tooth. Regen Med **4,** 377, 2009.

Address correspondence to:
Misako Nakashima, Ph.D.
Department of Dental Regenerative Medicine
Center of Advanced Medicine for Dental and Oral Diseases
National Center for Geriatrics and Gerontology
Research Institute
35 Gengo, Morioka
Obu, Aichi 474-8522
Japan

E-mail: misako@ncgg.go.jp

Received: October 23, 2010
Accepted: March 17, 2011
Online Publication Date: April 27, 2011

This article has been cited by:

1. Ryo Ishizaka, Koichiro Iohara, Masashi Murakami, Osamu Fukuta, Misako Nakashima. 2011. Regeneration of dental pulp following pulpectomy by fractionated stem/progenitor cells from bone marrow and adipose tissue. *Biomaterials* . [CrossRef]
2. F.J. Rodríguez-Lozano, J.M. Moraleda. 2011. Use of dental stem cells in regenerative dentistry: A possible alternative. *Translational Research* . [CrossRef]

TISSUE ENGINEERING: Part A
Volume 17, Numbers 9 and 10, 2011

DOI: 10.1089/ten.tea.2010.0306

Dental Pulp-Derived CD31$^-$/CD146$^-$ Side Population Stem/Progenitor Cells Enhance Recovery of Focal Cerebral Ischemia in Rats

Masahiko Sugiyama, D.D.S.,[1,2] Koichiro Iohara, Ph.D.,[1] Hideaki Wakita, Ph.D.,[3] Hisashi Hattori, Ph.D.,[2] Minoru Ueda, Ph.D.,[2] Kenji Matsushita, Ph.D.,[1] and Misako Nakashima, Ph.D.[1]

Regenerative therapy using stem cells is a promising approach for the treatment of stroke. Recently, we reported that CD31$^-$/CD146$^-$ side population (SP) cells from porcine dental pulp exhibit highly vasculogenic potential in hindlimb ischemia. In this study, we investigated the influence of CD31$^-$/CD146$^-$ SP cells after transient middle cerebral artery occlusion (TMCAO). Adult male Sprague-Dawley rats were subjected to 2 h of TMCAO. Twenty-four hours after TMCAO, CD31$^-$/CD146$^-$ SP cells were transplanted into the brain. Motor function and infarct volume were evaluated. Neurogenesis and vasculogenesis were determined with immunochemical markers, and the levels of neurotrophic factors were assayed with real-time reverse transcription–polymerase chain reaction. In the cell transplantation group, the number of doublecortin-positive cells increased twofold, and the number of NeuN-positive cells increased eightfold, as compared with the control phosphate-buffered saline group. The vascular endothelial growth factor level in the ischemic brain with transplanted cells was 28 times higher than that in the normal brain. In conclusion, CD31$^-$/CD146$^-$ SP cells promoted migration and differentiation of the endogenous neuronal progenitor cells and induced vasculogenesis, and ameliorated ischemic brain injury after TMCAO.

Introduction

Several preclinical studies have provided evidence that transplanted stem cells have therapeutic potential in the treatment of stroke.[1] Stem cells have the capability to migrate to areas of injury and secrete neuroprotective factors to induce neurogenesis.[2] In the adult mammalian brain, neurogenesis persists in certain distinct regions of the central nervous system such as the subventricular zone (SVZ) and the dentate gyrus of the hippocampus.[3] It has been reported that transplanting differentiated neural stem cells isolated from dental pulp improved motor disability and reduced infarct volume.[4] However, the influence of transplanting stem/progenitor cells isolated from dental pulp in cerebral ischemia has not been elucidated. Recently, we reported that CD31$^-$/CD146$^-$ side population (SP) cells containing stem/progenitor cells from porcine dental pulp exhibit highly vasculogenic potential *in vitro* and promote revascularization in hindlimb ischemia.[5] In the present study, we investigated the effects of these cells on neurogenesis and vasculogenesis in a cerebral ischemia model in a rat. In addition, the effects on the motor dysfunction and infarct volume were evaluated after transient middle cerebral artery occlusion (TMCAO).

Materials and Methods

Isolation of CD31$^-$/CD146$^-$ SP cells

CD31$^-$/CD146$^-$ SP and CD31$^+$/CD146$^-$ SP cells were isolated from porcine tooth germ, as described previously.[5] CD31$^-$/CD146$^-$ SP cells were cultured in endothelial basal medium-2 (EBM-2, single quots cc–4176) with 10 ng/mL insulin-like growth factor 1 (IGF1), 10 ng/mL epidermal growth factor (EGF), and 10% fetal bovine serum (FBS). CD31$^+$/CD146$^-$ SP cells were cultured in EBM-2 with 10 ng/mL bFGF, 10 ng/mL vascular endothelial growth factor (VEGF), 138 nM hydrocortisone, 0.09 mg/mL heparin, 50 μg/mL ascorbic acid, and 10% FBS. They were routinely subcultured up to 70% confluence under identical conditions.

Cerebral ischemia model

All animal experiments were approved by the Institutional Animal Care and Use Committee (National Center for the Geriatrics and Gerontology). Adult male Sprague-Dawley rats (Japan SLC, Inc.) weighing 300–400 g were used. Animals were initially anesthetized with 5% isoflurane (Abbott Laboratories) and maintained under anesthesia with 1.5% isoflurane in a mixture of 70% N_2O and 30% O_2. Rectal

[1]Department of Oral Disease Research, National Center for Geriatrics and Gerontology, Research Institute, Obu, Aichi, Japan.
[2]Department of Oral and Maxillofacial Surgery, Laboratory Medicine, Nagoya University Graduate School of Medicine, Nagoya, Japan.
[3]Department of Vascular Dementia Research, National Center for Geriatrics and Gerontology, Research Institute, Obu, Aichi, Japan.

temperature was maintained at 37°C±0.5°C on a heating pad. Focal cerebral ischemia was induced by TMCAO with 2 h.[6] A 4-0 monofilament nylon suture (Shirakawa) with the tip rounded by flame heating and silicone (KE-200; Shin-Etsu Chemical) was advanced from the external carotid artery into the internal carotid artery until it blocked the origin of the MCA. Two hours after occlusion, reperfusion was performed by withdrawal of the suture. The regional cerebral blood flow of the MCA territory was measured using a laser-Doppler flowmeter (Omega FLO-N1; Omega Wave, Inc.) after occlusion. The response was considered positive and included only if the reduction in regional cerebral blood flow was >70%.

Transplantation

Twenty-four hours after TMCAO (day 0), the rats were again anesthetized with sodium pentobarbital (Schering-Plough) (0.25 mL/kg, intraperitoneally) and maintained under anesthesia with 1.5% isoflurane in a mixture of 70% N_2O and 30% O_2. Animals were randomly divided into three groups: (I) $CD31^-/CD146^-$ SP cell transplantation group ($n=24$, day 3 sacrificed=6, day 9 sacrificed=7, day 21 sacrificed=11), (II) unfractionated pulp cell transplantation group ($n=4$, used for motor function), and (III) vehicle alone (phosphate-buffered saline [PBS]) group ($n=20$, day 3 sacrificed=6, day 9 sacrificed=5, day 21 sacrificed=9). The infarction site was targeted for transplantation at the striatum of the following coordinates: 1.0 mm rostral to the bregma, 6.0 mm lateral to the midline, 5.0 mm ventral to the dura (Fig. 1A, B). Subsequently, 1×10^6 $CD31^-/CD146^-$ SP cells or unfractionated pulp cells at the fifth to seventh passage after labeling with 1,1-dioctadecyl-3,3,3,3 tetramethylindocarbocyanine perchlorate (DiI; Sigma), and removing all added factors into each medium were diluted with 2 μL of PBS, and were transplanted by Hamilton microsyringe (Hamilton). The control group consisted of an equal volume of PBS injected into the same site.

Immunohistochemistry

At day 3 or 21 after injection, the rat was transcardially perfused with 4% paraformaldehyde solution (Nakarai Tesque). The brain was removed and postfixed in paraformaldehyde. The following day, it was immersed in 30% sucrose solution. Twelve-micrometer-thick coronal sections were cut on a cryostat. For immunohistochemistry, the sections were preincubated in blocking solution (PBS containing 5% normal serum of the species in which the secondary antibody was raised) for 2 h at room temperature, and incubated with primary antibodies diluted for 1 h at room temperature. The primary antibodies were as follows: neuronal progenitor cells (NPC) marker, rabbit anti-doublecortin (1:50; Abcam, Inc.); neuron marker, rabbit anti-neurofilament H (1:200; Chemicon) and mouse anti-NeuN (anti-neuronal nuclei, 1:500; Chemicon); endothelial cell marker, mouse anti-RECA1 (rat endothelial cell antigen; Monosan); apoptosis marker, rabbit anti-cleaved caspase-3 (1:50; Cell Signaling Technology, Inc.); and VEGF marker, rabbit anti-VEGF (VEGF [P-20]: sc-1836; Santa Cruz Biotech). After washing, sections were incubated for 1 h at room temperature with secondary antibodies (on day 21, for neurofilament H/doublecortin, Donkey anti-rabbit IgG FITC [1:400; Jackson ImmunoResearch]; for NeuN/RECA1, Goat anti-mouse IgG FITC [1:200; MP Biomedicals]; and for VEGF, rabbit anti-goat

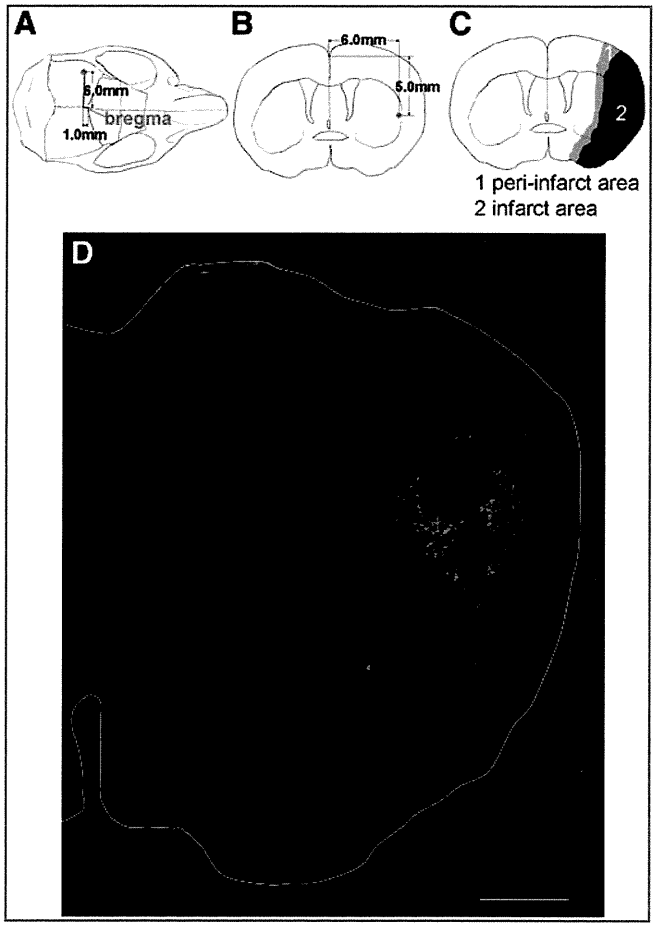

FIG. 1. **(A)** Overhead and **(B)** coronal view of the injection site. **(C)** The peri-infarct area. Peri-infarct area (gray), infarct core (black). **(D)** DiI-labeled transplanted $CD31^-/CD146^-$ SP cells (red) migrated from the original injection site to the peri-infarct area in the cortex and striatum. White outline is the outer circumference of brain. Scale bar=1000 μm. SP, side population. DiI, 1,1-dioctadecyl-3,3,3,3 tetramethylindocarbocyanine perchlorate. Color images available online at www.liebertonline.com/tea

IgG-HRP [1:400; Invitrogen Corporation]. On day 3, for cleaved caspase-3, goat anti-rabbit IgG-HRP [1:400; Invitrogen] and for VEGF, rabbit anti-goat IgG-HRP [1:400; Invitrogen]). The sections with HRP-conjugated secondary antibodies were incubated in anti-fluorescein-HRP (1:400; TSA™ Fluorescence Systems; PerkinElmer) for 7 min at room temperature. Adjacent sections were used as negative controls. In the control sections, all procedures were processed in the same manner except that the primary antibodies were omitted. To identify migration of NPC from SVZ, we observed the cryosections on days 9 and 21 with anti-doublecortin on fluorescence microscope (BZ-9000; Keyence) and BZ-HIC (Keyence).

Statistical analyses of the density of cells

The density of NPCs, neurons, endothelial cells, and apoptotic cells in the peri-infarct area (Fig. 1C) and the contralateral region in the $CD31^-/CD146^-$ SP cell transplantation group and PBS groups were determined. In all groups (PBS group, $CD31^-/CD146^-$ SP cell transplantation group,

TABLE 1. PORCINE PRIMERS FOR REAL-TIME REVERSE TRANSCRIPTION–POLYMERASE CHAIN REACTION AND *IN SITU* HYBRIDIZATION

Gene		*5′ DNA sequence 3′*	*Product size (bp)*	*Accession no.*
r.β-actin	Forward	AAGTACCCCATTGAACACGG	257	NM_031144
	Reverse	ATCACAATGCCAGTGGTACG		
p.β-actin	Forward	CTGGGGCCTAACGTTCTCAC	198	BI118314
	Reverse	GTCCTTTCTTCCCCGATGTT		
VEGF	Forward	ATGGCAGAAGGAGACCAGAA	224	MN_214084
	Reverse	ATGGCGATGTTGAACTCCTA		
BDNF	Forward	TTCAAGAGGCCTGACATCGT	180	MN_214259
	Reverse	AGAAGAGGAGGCTCCAAAGG		
NGF	Forward	TGGTGTTGGGAGAGGTGAAT	210	L31889
	Reverse	CCGTGTCGATTCGGATAAA		
GDNF	Forward	ACGGCCATACACCTCAATGT	144	GU229658
	Reverse	CCGTCTGTTTTTGGACAGGT		

BDNF, brain-derived neurotrophic factor; GDNF, glial cell line-derived neurotrophic factor; NGF, nerve growth factor; VEGF, vascular endothelial growth factor.

and contralateral group, $n=3$), each five sections at every 120-μm were stained with doublecortin, NeuN, RECA1, and cleaved caspase-3. The microscopic images were scanned and five typical frames (0.49 mm^2) were measured for each section. Thus, 75 frames on an average were determined per group. The positively stained area relative to total area (7.41 mm^2) was statistically analyzed using a Dynamic cell count, BZ-HIC (Keyence).

Real-time reverse transcription–polymerase chain reaction

Total RNA on cryosamples was extracted using Trizol (Invitrogen) from the area of the DiI-positive cells observed in the section. First-strand cDNA syntheses were performed from total RNA by reverse transcription with ReverTra Ace-α (Toyobo). Real-time reverse transcription–polymerase chain reaction (RT-PCR) amplifications were performed at 95°C for 10 s, at 62°C for 15 s, and at 72°C for 8 s using the porcine-specific primers *VEGF*. The specificity of the primers to porcine was confirmed by no amplification of the first-strand cDNA from rats with normal brains. The RT-PCR products were subcloned into a pGEM-T Easy vector (Promega) and confirmed by DNA sequencing based on published cDNA sequences. Gene expression of the transplanted cells in the infarct area was compared with that in the porcine normal brain tissue and that in transplanted cells in the normal brain after normalizing with β-actin.

In situ *hybridization*

Neurotrophic factors expressed in $CD31^-/CD146^-$ SP cells were examined with *in situ* hybridization in cryosections on day 21. Porcine cDNA of *VEGF* (224 bp), glial cell line-derived neurotrophic factor (*GDNF*; 144 bp), brain-derived neurotrophic factor (*BDNF*;180 bp), and nerve growth factor (*NGF*; 210 bp) were linearized with *Nco*I, *Spe*I, *Nco*I, and *Spe*I, respectively, for anti-sense probes, and linearized with *Spe*I, *Nco*I, *Spe*I, and *Nco*I, respectively, for sense probes. The *VEGF* probe was constructed from plasmids after subcloning the PCR products using the same primers designed for real-time RT-PCR. The *GDNF*, *BDNF*, and *NGF* probes were also constructed in same way as the *VEGF* probe. Since a published porcine *GDNF* sequence was not available, human primers for *GDNF* (forward 5′-TATGGGATGTCGT GGCTGT-3′, reverse 5′-TCCACACCTTTTAGCGGAAT-3′) were used for cDNA subcloning of porcine *GDNF* (630 bp). The design of the oligonucleotide primers (Table 1) was based on both published porcine cDNA sequences and the newly cloned cDNA sequence of the porcine *GDNF*. The four probes were labeled with DIG (Invitrogen) and the DIG signals were detected with TSA system FITC-conjugated tyramide (Invitrogen).

Migration, proliferation, and anti-apoptotic assays

At 50% confluence, the culture medium was switched to serum-free EBM-2. The conditioned medium (CM) from $CD31^-/CD146^-$ SP cells, $CD31^+/CD146^-$ SP cells, and unfractionated pulp cells were collected after 48 h.

For migration assay, modified Boyden chamber assays were performed with polyethylene terephthalate membrane (BD Bioscience) in a 24-well plate (BD Bioscience). SHSY5Y cells (Sanyo Chemical Industries, Ltd.) (1×10^5 cells/well) were seeded on the insert polyethylene terephthalate membrane, and 500 μL of DMEM-F12 (Sigma) with 20% of the three CMs was, respectively, poured into the tissue culture 24-well plate. SHSY5Y cells were derived from a neural crest tumor of early childhood, predominantly composed of undifferentiated neuroblast-like cells.[7] After 24 h, the SHSY5Y cells passing through the membrane were counted after detaching them with 0.05% trypsin–0.02% EDTA.

For cell proliferation assay, SHSY5Y cells (1×10^3/96-well plate) were cultured in DMEM-F12 containing 10% FBS for 24 h, and subsequently in serum-free DMEM-F12 containing 0.2% bovine serum albumin for further 24 h. Then, the medium was changed into each DMEM-F12 containing 0.02% FBS with 20% of three CMs. Ten micrometers of Tetra-color one (Seikagaku Kogyo, Co.) was added to the 96 well-plate, and cell numbers were measured by spectrophotometry at 450 nm at 2, 12, 24, 36, and 48 h of culture.

For the anti-apoptotic assay, SHSY5Y cells were cultured in DMEM-F12 in a 35-mm dish for 2 days and then incubated with 300 nM staurosporine[8] (Sigma) in DMEM-F12 with 20% of the three CMs. After 24 h, SHSY5Y were harvested, and

the cell suspensions were treated with Annexin V-FITC (Roche Diagnostics) and PI for 15 min, and analyzed by flow cytometry JSAN.

BDNF (Peprotech), GDNF (Peprotech), VEGF-A (Peprotech), or NGF (Peprotech) at 50 ng/mL was used as a control for the three assays.

Evaluation of motor disability

Rats were blindly examined on days 0, 2, 6, and 9 with a standardized motor disability scale by slight modifications.[9] Rats were scored 1 point for each of the following parameters: flexion of the forelimb contralateral to the stroke when instantly hung by the tail, extension of the contralateral hind limb when pulled from the table, and rotation to the paretic side against resistance. In addition, 1 point was scored for circling motion to the paretic side when trying to walk, 1 point was scored for failure to walk out of a circle of 50 cm in diameter within 10 s, 2 points were scored for failure to leave the circle within 20 s, and 3 points were scored for inability to exit the circle within 60 s. In addition, 1 point each was scored for inability of the rat to extend the paretic forepaw when pushed against the table from above, laterally, and sideways. The motor disability scale was performed 3 times per animal time-point.

Assessment of infarct volume

The cryosections obtained from samples on days 3 and 21 were stained with hematoxylin and eosin.[10] ImageJ (National Institutes of Health) was used to determine each infarct area in 9 coronal sections in 12-μm thickness at 0.84-mm intervals. All of the infarction area was covered by these nine coronal sections. Regional infarct volumes were calculated by summing the infarct areas and multiplying these areas by the distance between sections (0.84 mm), followed by remediation for brain edema.[11]

Statistical analyses

Data are reported as means ± SD. p-Values were calculated using the unpaired Student's t-test.

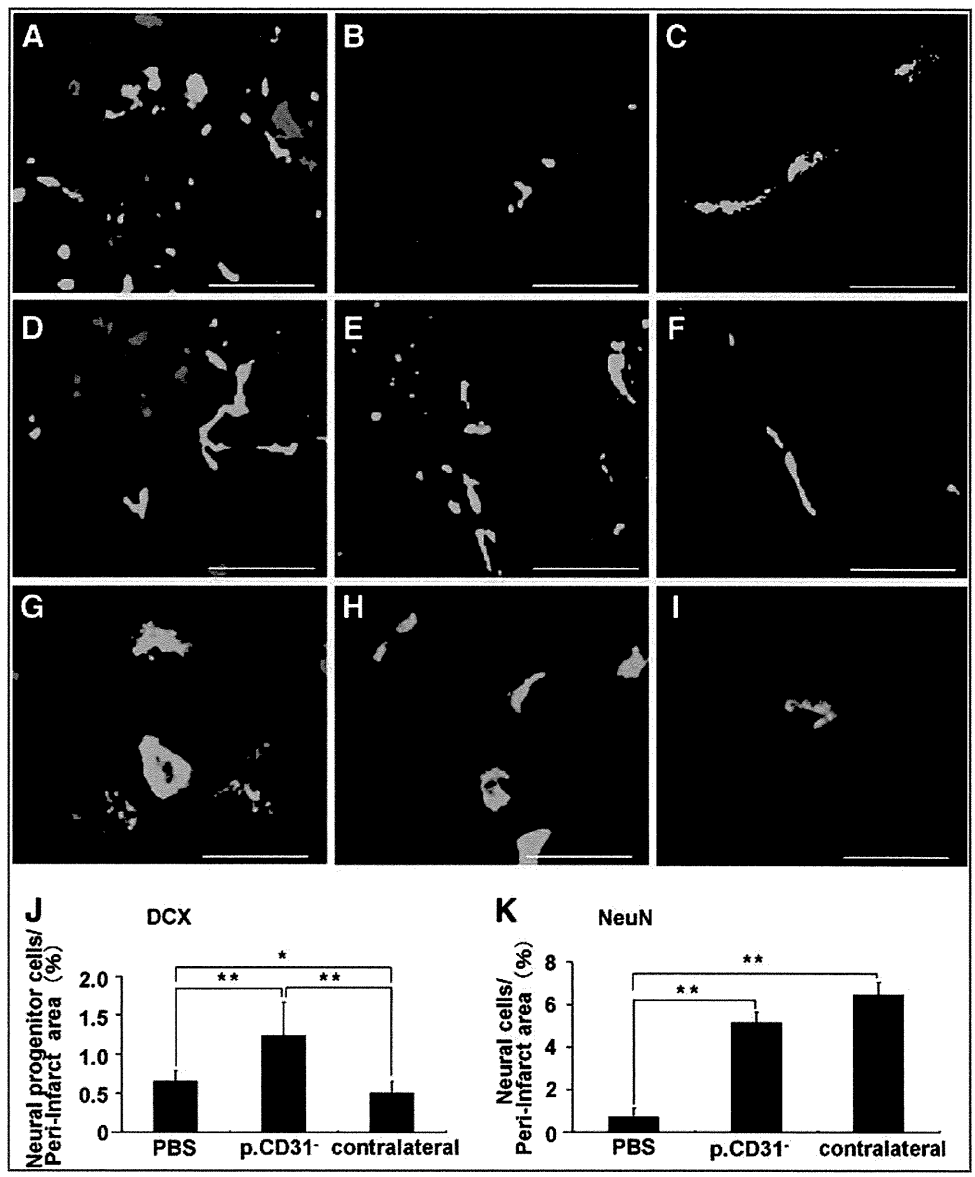

FIG. 2. Doublecortin-positive cells (green: **A–C**), Neurofilament-positive cells (green: **D–F**), and NeuN-positive cells (green: **G–I**). $CD31^-/CD146^-$ SP cells (red) transplantation group of the ipsilateral **(A, D, G)** and the contralateral **(B, E, H)** on day 21. PBS group **(C, F, I)** on day 21. Statistical analyses of density of NPCs **(J)** and neurons **(K)** on day 21. Scale bars = 20 μm. $*p < 0.005$, $**p < 0.001$, Student's t-test. Each point is expressed as mean ± SD of 75 determinations. NPC, neuronal progenitor cells; PBS, phosphate-buffered saline. Color images available online at www.liebertonline.com/tea

Results

Pulp stem cell outcome

DiI-labeled transplanted $CD31^-/CD146^-$ SP cells were characterized by round-to-oval nuclei with minimal variable cytoplasm. The transplanted cells survived and migrated from the original injection site to peri-infarct area in the cortex and striatum (Fig. 1D).

Transplanted cells localized in proximity of doublecortin (Fig. 2A) and neurofilament (Fig. 2D) or NeuN-positive cells (Fig. 2G) on day 21. Few doublecortin cells were observed in the contralateral side (Fig. 2B). There was a twofold increase in doublecortin-positive cells (Fig. 2J) and an eightfold increase in NeuN-positive cells (Fig. 2K) on day 21 in the $CD31^-/CD146^-$ SP cell transplantation group compared with that in the PBS group. No evidence of differentiation of $CD31^-/CD146^-$ SP cells into neurons or endothelial cells was detected. The migration of NPCs with doublecortin from SVZ to the peri-infarct area was observed on days 9 and 21. The migration on day 9 was more prominent (Fig. 3I, K, M). These results suggest that the transplanted cells support the migration and differentiation of the NPCs. The number of

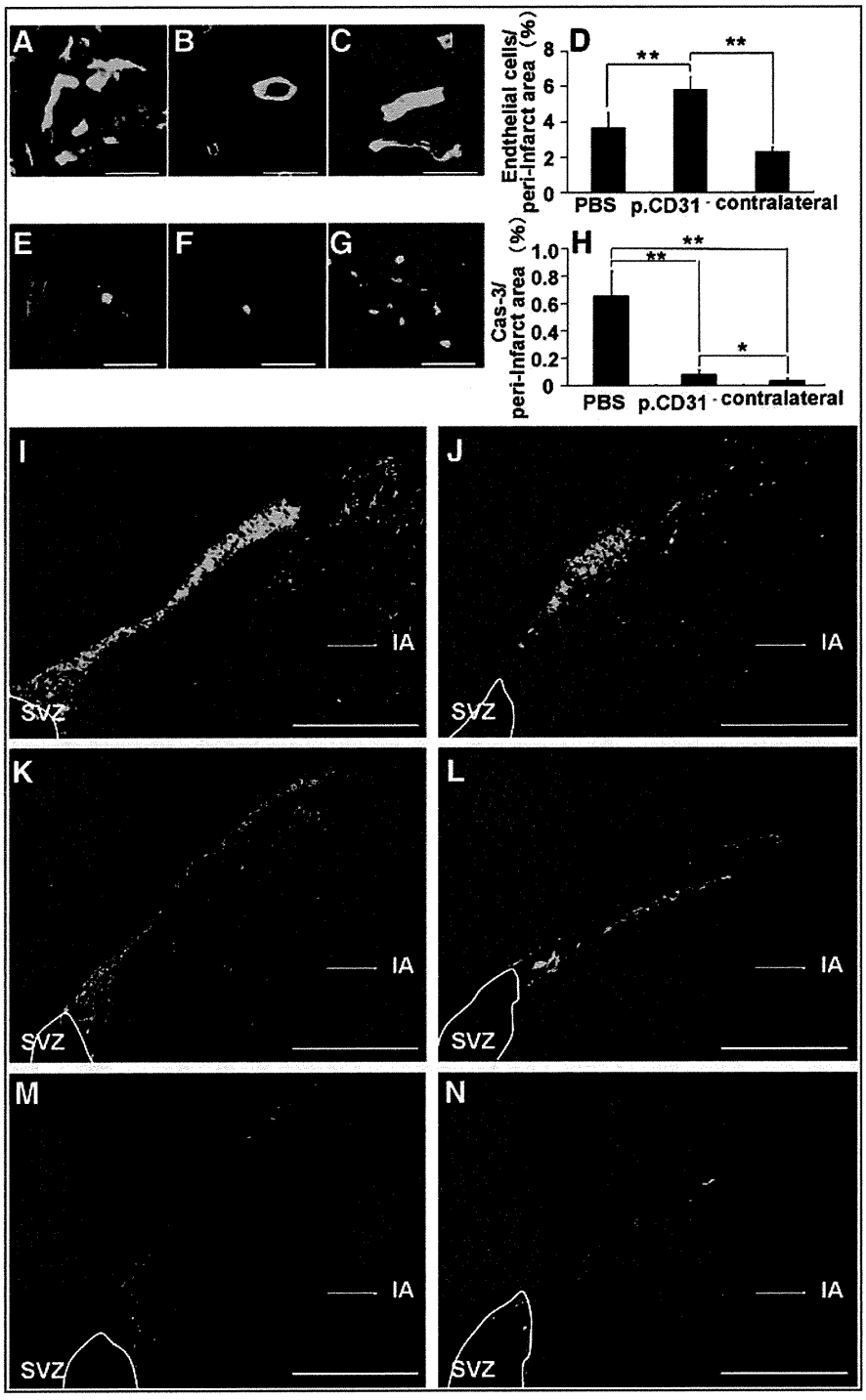

FIG. 3. RECA1-positive cells on day 21 (green: **A–C**) and cleaved caspase-3-positive cells on day 3 (green: **E–G**). $CD31^-/CD146^-$ SP cells (red) transplantation group of the ipsilateral **(A, E)** and the contralateral **(B, F)**. PBS group **(C, G)**. Statistical analyses of density of endothelial cells on day 21 **(D)** and cleaved caspase-3-positive cell on day 3 **(H)**. The migration of NPC from the SVZ to the peri-infarct area on days 9 **(I, J, M)** and 21 **(K, L, N)**. $CD31^-/CD146^-$ SP cells group **(I, J)**. Unfractionated pulp cells **(K, L)**. PBS group **(M, N)**. Scale bar = 20 μm **(A–C, E–G)**, and 300 μm **(I–N)**. $^*p < 0.01$, $^{**}p < 0.001$, Data were expressed as means ± SD at 75 determinations. The statistical difference was calculated by Student's *t*-test. IA, infarct area; SVZ, subventricular zone. Color images available online at www.liebertonline.com/tea

RECA1-positive cells on day 21 was increased in the CD31$^-$/CD146$^-$ SP cell transplantation group compared with that in the PBS group (Fig. 3D), indicating that the transplanted cells also promote angiogenesis after ischemia. In the CD31$^-$/CD146$^-$ SP cell transplantation group (Fig. 3H), there was a decrease in cleaved caspase-3-positive cells, suggesting that the transplanted cells have an anti-apoptotic function.

Expression of neurotrophic factors

The expression of several neurotrophic factors *VEGF*, *GDNF*, *NGF*, and *BDNF* was detected with *in situ* hybridization in the DiI-labeled CD31$^-$/CD146$^-$ SP cells in the peri-infarct area on day 21 (Fig. 4A–D). Real-time RT-PCR analysis demonstrated that expression of *VEGF* mRNA by the transplanted CD31$^-$/CD146$^-$ SP cells in the ischemic region on day 21 was 1,000 times and 28 times higher than that of normal porcine brain and that of the transplanted CD31$^-$/CD146$^-$ SP cells into normal rat striatum, respectively (Fig. 4E, F). Immunohistochemistry of VEGF showed that the VEGF protein was highly expressed in the DiI-labeled CD31$^-$/CD146$^-$ SP cells in the peri-infarct area on day 3 (Fig. 4G) compared with that on day 21 (Fig. 4H).

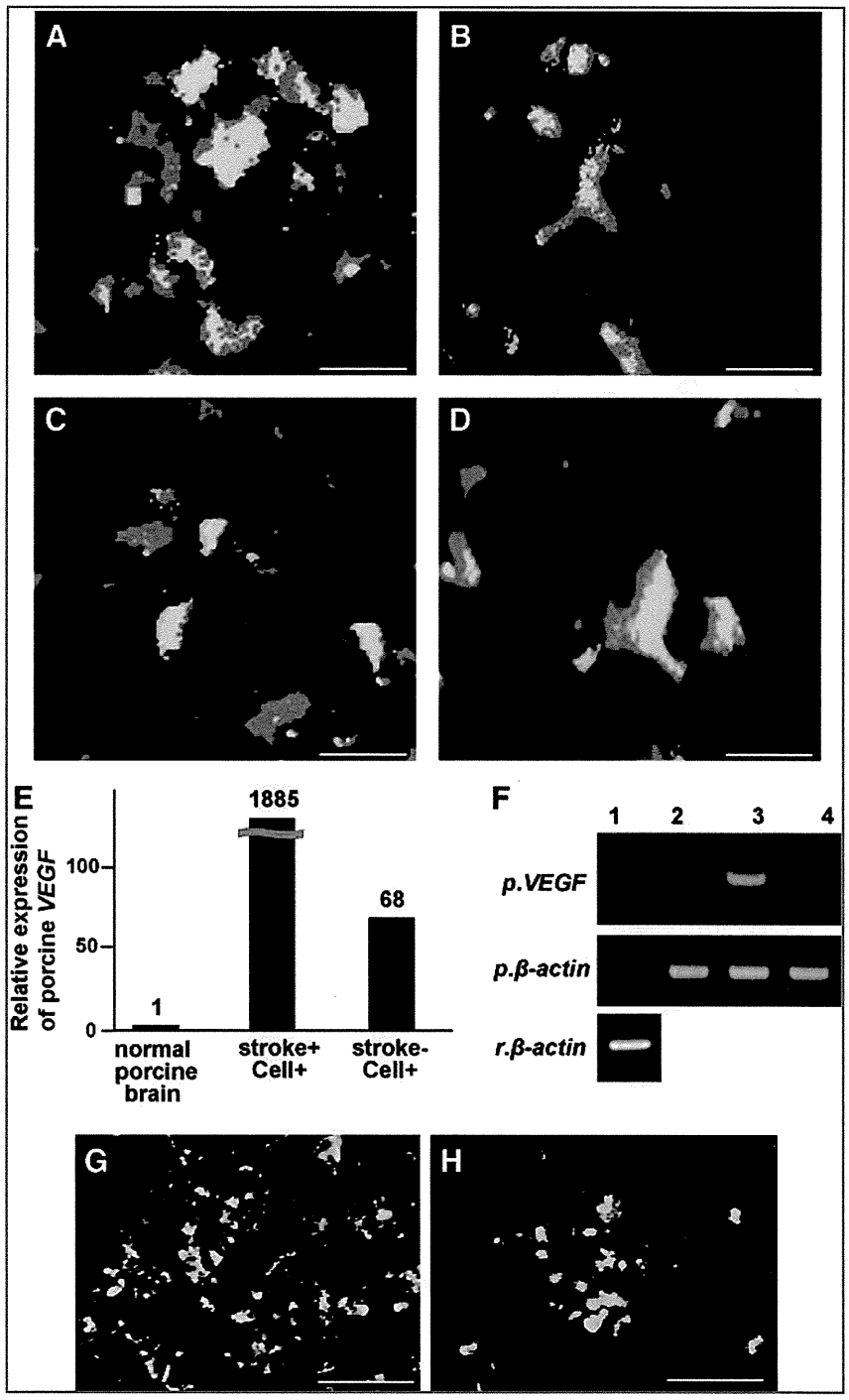

FIG. 4. Analysis of expression of *VEGF* **(A)**, *GDNF* **(B)**, *BDNF* **(C)**, and *NGF* **(D)** (green: **A–D)** of DiI-labeled transplanted CD31$^-$/CD146$^-$ SP cells (red) by *in situ* hybridization in the peri-infarct area. Real-time reverse transcription–polymerase chain reaction analysis of porcine *VEGF* (*pVEGF*) using porcine-specific primers **(E)**. Expression of porcine *VEGF* and porcine-specific and rat-specific β-actin 1, normal rat brain; 2, normal porcine brain; 3, peri-infarct area 21 days after transplantation of CD31$^-$/CD146$^-$ SP cells; 4, normal rat striatum 21 days after transplantation of the cells **(F)**. VEGF-positive cells on day 3 **(G)** and on day 21 **(H)** by immunohistochemistry. Scale bars = 10 μm **(A–D)** and 100 μm **(G, H)**. BDNF, brain-derived neurotrophic factor; GDNF, glial cell line-derived neurotrophic factor; NGF, nerve growth factor; VEGF, vascular endothelial growth factor. Color images available online at www.liebertonline.com/tea

Migration, proliferation, and anti-apoptotic assays

CM of CD31$^-$/CD146$^-$ SP cells showed higher migratory effect on SHSY5Y cells than VEGF, NGF, and BDNF, and was similar to GDNF (Fig. 5A). Its proliferation effect was higher than VEGF and NGF, and similar to BDNF and GDNF (Fig. 5B). Its anti-apoptotic activity was higher than BDNF, GDNF, and VEGF (Fig. 5C).

Evaluation of motor function

All groups (CD31$^-$/CD146$^-$ SP cells, unfractionated pulp cells, and PBS) displayed high score for motor function at the early stage (day 0, scores are 8.08±0.79; 8.25±0.96; 8.42±0.79, and day 2, 5.08±0.90; 6.25±1.26; 7.67±0.78, respectively). Progressive improvement in motor disability in the CD31$^-$/CD146$^-$ SP cell transplantation group after day 2 became significant on day 6 compared with PBS control group (2.67±1.23; 6.83±0.72), and more significant on day 9 compared with the unfractionated pulp cells and the PBS control group (1.33±0.78; 2.8±0.96; 6.50±0.67) (Fig. 6A). Persistent improvement in CD31$^-$/CD146$^-$ SP cells transplantation group was noted on day 14 (1.00±0.71) and 21 (0.80±0.45), whereas persistent impairment of motor disability (score above 4) was observed in the PBS group on day 14 (5.60±0.55) and 21 (5.40±0.59) (Fig. 6A). Further, the video image demonstrated significant recovery in motor function of the CD31$^-$/CD146$^-$ SP cell transplantation group compared with the unfractionated pulp cells and PBS control groups on day 6 (Supplementary Videos S1–S3; Supplementary Data are available online at www.liebertonline.com/tea).

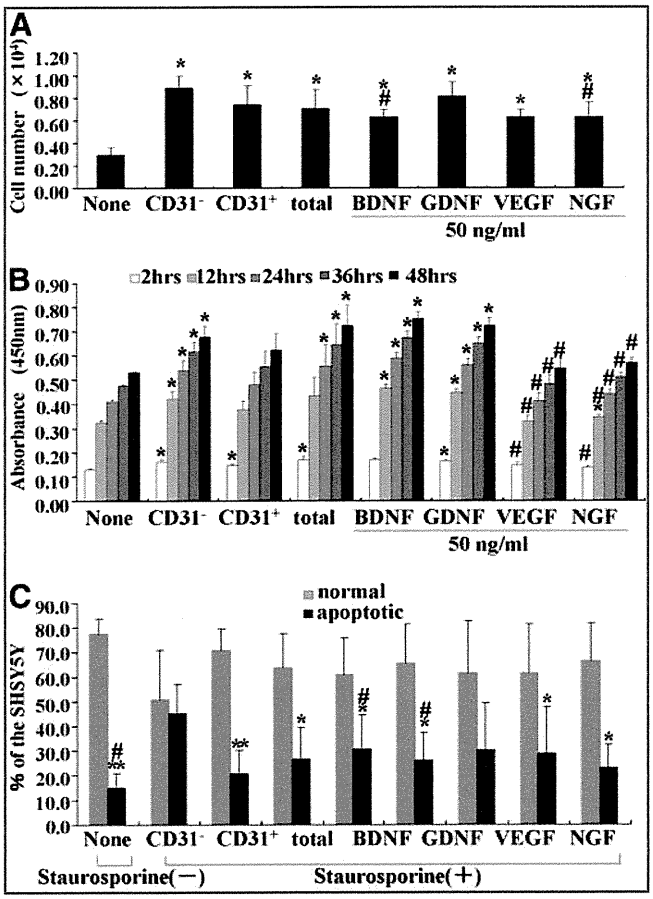

FIG. 5. The migration **(A)**, proliferative effect **(B)**, and anti-apoptotic effect **(C)** of conditioned medium of CD31$^-$/CD146$^-$ SP cells, CD31$^+$/CD146$^-$ SP cells, and unfractionated total pulp cells and neurotrophic factors on SHSY5Y cells. $^*p<0.05$, $^{**}p<0.005$, versus control. $^\#p<0.05$, versus CD31$^-$/CD146$^-$ SP cells. Data were expressed as means±SD at three determinations **(A, C)** and four determinations **(B)**. Student's *t*-test.

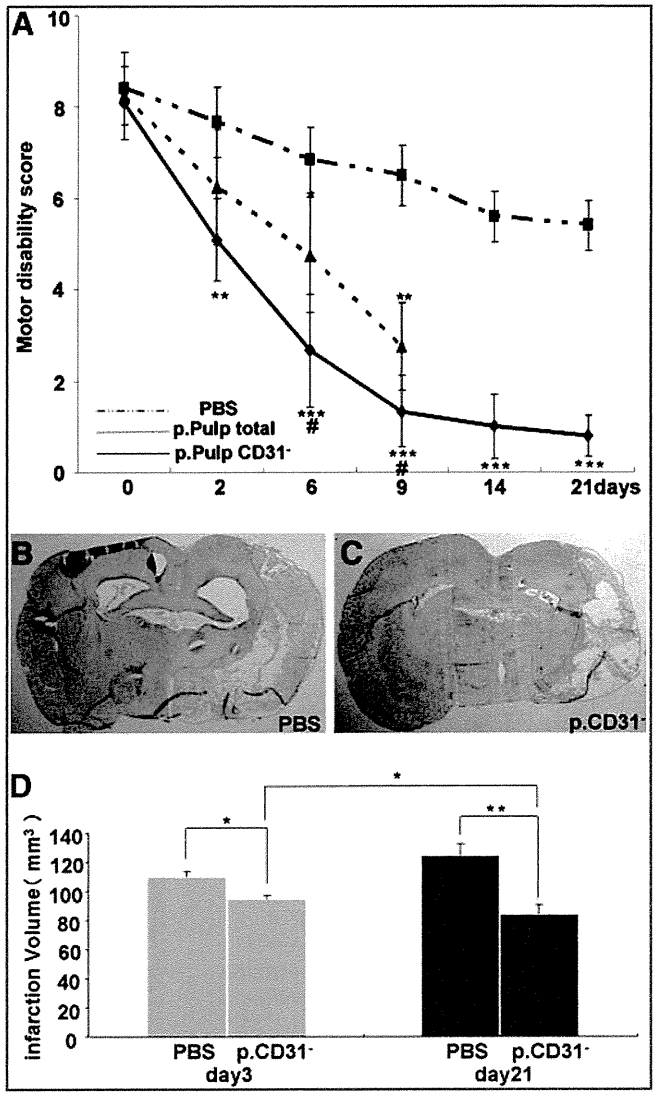

FIG. 6. Motor disability test by injection of the CD31$^-$/CD146$^-$ SP cells, the unfractionated pulp cells and the PBS on days 0, 2, 6, and 9 **(A)**. Infarct area on day 21 **(B, C)**. The reduction of the infarct volume 3 and 21 days after injection of CD31$^-$/CD146$^-$ SP cells **(D)**. $^*p<0.05$, $^{**}p<0.005$, $^{***}p<0.001$, versus control. $^\#p<0.05$, versus CD31$^-$/CD146$^-$ SP cells. Data were expressed as means±SD at three determinations **(D)**, Student's *t*-test.

Reduction of infarct volume

There was a significant decrease in the infarct volume on days 3 and 21 in the CD31$^-$/CD146$^-$ SP cell transplantation

group (day 3, $95.2 \pm 2.5\,mm^3$, $n=3$: day 21, $84.7 \pm 6.5\,mm^3$, $n=4$) compared to PBS group (day 3, $109.7 \pm 4.1\,mm^3$, $n=3$: day 21, $123.9 \pm 7.4\,mm^3$, $n=4$). The difference of infarct volume between the $CD31^-/CD146^-$ SP cell transplantation group and the PBS group increased over time (reduced by 13.3% on day 3 and reduced by 32.9% on day 21) (Fig. 6D). These results suggest that transplanted $CD31^-/CD146^-$ SP cells promoted the regeneration.

Discussion

In the current study, we demonstrated that transplanted $CD31^-/CD146^-$ SP cells migrated to the peri-infarct area. In addition, these cells released neurotrophic factors, and promoted migration and differentiation of the endogenous NPCs in SVZ. They also induced vasculogenesis in the peri-infarct area. These results indicate that $CD31^-/CD146^-$ SP cells ameliorated the ischemic tissue injury and accelerated the functional recovery after TMCAO. We have hypothesized that three mechanisms may contribute to the actions of VEGF. First, VEGF produced by transplanted cells may promote neurogenesis. NPCs in SVZ are known to migrate to the peri-infarct area and differentiate into neurons.[1] In this study, VEGF induced a chemotactic response in SHSY5Y cells. The transplanted $CD31^-/CD146^-$ SP cells migrated to the peri-infarct area and expressed VEGF. These results suggest that VEGF released by $CD31^-/CD146^-$ SP cells in the peri-infarct may promote migration of the endogenous NPCs in SVZ. Second, VEGF produced by transplanted cells may promote vasculogenesis. VEGF binds to its receptors on locally present vascular endothelial cells and directly initiates the angiogenic response.[12] In this study, the number of RECA1-positive endothelial cells significantly increased in the cell transplantation group. Third, VEGF may provide a neuroprotective effect. The neuroprotective effects of VEGF in experimental cerebral ischemia have been reported.[13] In cell the transplantation group, the number of cleaved caspase-3-immunopositive cells in the peri-infarct area was decreased compared with that in the PBS group, thus demonstrating the anti-apoptotic effects of VEGF on SHSY5Y cells. These results suggest that VEGF produced by $CD31^-/CD146^-$ SP cells may inhibit apoptosis of neurons. Thus, VEGF demonstrates pleiotropic effects on neurogenesis, vasculogenesis, and neuroprotection.

As VEGF is a potent vascular permeability factor, it may accelerate brain edema after stroke. Administration of VEGF in early ischemia (1 h after ischemia) leads to significant increase in blood–brain barrier leakage as well as enlarged ischemic areas.[14] However, VEGF administration at 24 h after TMCAO reduces infarct size, improves neurologic recovery, enhances neurogenesis in the SVZ and angiogenesis in the ischemic border zone.[14] In this study, $CD31^-/CD146^-$ SP cells were transplanted 24 h after TMCAO and we monitored the reduction of infarct size and improvement of motor disability. The time of administration of cells is critical. Thus, if $CD31^-/CD146^-$ SP cells were transplanted during an optimal window of time, they exhibit beneficial effects without the deleterious effects of edema.

In addition, $CD31^-/CD146^-$ SP cells expressed other neurotrophic factors such as GDNF,[15] NGF,[16] and *BDNF*[16] in the peri-infarct area. These neurotrophic factors had migratory, proliferative, and/or anti-apoptotic effects on SHSY5Y cells *in vitro* and may also contribute to the recovery from ischemic brain injury.

Finally, we explored the plausible underlying mechanisms of how injection of $CD31^-/CD146^-$ SP cells into the brains of immunocompetent rats staved off graft rejection. Blood–brain barrier is known to play a critical role in maintaining the immune-privileged status of the central nervous system.[17] It is well known that mesenchymal stem cells from bone marrow are not rejected by hosts and immunosuppression is not required in rodents.[1] Dental pulp stem cells have many similarities to mesenchymal stem cells; transplanted $CD31^-/CD146^-$ SP cells possess immunosuppressive properties.[18]

Conclusion

In summary, the transplantation of porcine $CD31^-/CD146^-$ SP cells promotes neurogenesis and vasculogenesis in an induced peri-infarct area, and enhances recovery after TMCAO in rats. Further research is needed to understand the underlying mechanisms. For potential clinical application and translational studies, the safety of $CD31^-/CD146^-$ SP cells must be assessed, including tumor formation. In conclusion, regeneration therapy using $CD31^-/CD146^-$ SP cells is a potential candidate in the treatment of stroke.

Acknowledgments

The authors thank Drs. Masataka Ito, Kayo Adachi, and Kiyomi Imabayasghi for their assistance. This work was supported by funds from Collaborative Development of Innovative Seeds, Potentiality verification stage from Japan Science and Technology Agency, a Grant-in-Aid for Scientific Research from the Ministry of Education, Science, Sports and Culture, Japan, No. 19659499 (M.N.), No. 20390504 (M.N.), and No. 18592173 (H.H.), and the Research Grant for Longevity Sciences (19C-2, 21A-7) from the Ministry of Health, Labour, and Welfare (M.N.).

Disclosure Statement

No competing financial interests exist.

References

1. Burns, T.C., Verfaillie C.M., and Low W.C. Stem cells for ischemic brain injury: a critical review. J Comp Neurol **515,** 125, 2009.
2. Locatelli, F., Bersano, A., Ballabio, E., Lanfranconi, S., Papadimitriou, D., Strazzer, S., Bresolin, N., Comi, G.P., and Corti, S. Stem cell therapy in stroke. Cell Mol Life Sci **66,** 757, 2009.
3. Gage, F.H., Kempermann, G., Palmer, T.D., Peterson, D.A., and Ray, J. Multipotent progenitor cells in the adult dentate gyrus. J Neurobiol **36,** 249, 1998.
4. Yang, K.L., Chen, M.F., Liao, C.H., Pang, C.Y., and Lin, P.Y. A simple and efficient method for generating Nurr1-positive neuronal stem cells from human wisdom teeth (tNSC) and the potential of tNSC for stroke therapy. Cytotherapy **11,** 606, 2009.
5. Iohara, K., Zheng, L., Wake, H., Ito, M., Nabekura, J., Wakita, H., Nakamura, H., Into, T., Matsushita, K., and Nakashima, M. A novel stem cell source for vasculogenesis in ischemia: subfraction of side population cells from dental pulp. Stem Cells **26,** 2408, 2008.

6. Longa, E.Z., Weinstein, P.R., Carlson, S., and Cummins, R. Reversible middle cerebral artery occlusion without craniectomy in rats. Stroke **20,** 84, 1989.
7. Koning, G., Colin, L., and Beyreuther, K. Retionic acid induced differentiated neuroblastoma cells show increased expression of the βA4 amyloid gene of Alzheimer's disease and an altered splicing pattern. FEBS Lett **269,** 305, 1990.
8. Richard, B., Eric, S., Patrick, O., Kurt, W., and Ywes, P. Induction of a common pathway of apoptosis by staurosporine. Exp Cell Res **211,** 314, 1994.
9. Leker, R.R., Gai, N., Mechoulam, R., and Ovadia, H. Drug-induced hypothermia reduces ischemic damage: effects of the cannabinoid HU-210. Stroke **34,** 2000, 2003.
10. Ginsberg, M.D. Adventures in the pathophysiology of brain ischemia: penumbra, gene expression, neuroprotection: the 2002 Thomas Willis Lecture. Stroke **34,** 214, 2003.
11. Leach, M.J., Swan, J.H., Eisenthal, D., Dopson, M., and Nobbs, M. BW619C89, a glutamate release inhibitor, protects against focal cerebral ischemic damage. Stroke **24,** 1063, 1993.
12. Plate, K.H., Beck, H., Danner, S., Allegrini, P.R., and Wiessner, C. Cell type specific upregulation of vascular endothelial growth factor in an MCA-occlusion model of cerebral infarct. J Neuropathol Exp Neurol **58,** 654, 1999.
13. Jin, K.L., Mao, X.O., and Greenberg, D.A. Vascular endothelial growth factor: direct neuroprotective effect in *in vitro* ischemia. Proc Natl Acad Sci U S A **97,** 10242, 2000.
14. Heike, B., and Karl, H.P. Angiogenesis after cerebral ischemia. Acta Neuropathol **117,** 481, 2009.
15. Leu-Fen, H., Lin, H., Doherty, D., Lile, B., and Frank, C. GDNF: a glial cell line-derived neurotrophic factor for midbrain dopaminergic neurons. Science **260,** 1072, 1993.
16. Shawne, N., Fernando, G., James, C., and Carl, C. Physical activity increases mRNA for brain-derived neurotrophic factor and nerve growth factor in rat brain. Brain Res **726,** 49, 1996.
17. Pachter, J.S., De Vries, H.E., and Fabry, Z. The blood-brain barrier and its role in immune privilege in the central nervous system. J Neuropathol Exp Neurol **62,** 593, 2003.
18. Pierdomenico, L., Bonsi, L., Calvitti, M., Rondelli, D., Arpinati, M., Chirumbolo, G., Becchetti, E., Marchionni, C., Alviano, F., Fossati, V., Staffolani, N., Franchina, M., Grossi, A., and Bagnara, G.P. Multipotent mesenchymal stem cells with immunosuppressive activity can be easily isolated from dental pulp. Transplantation **80,** 836, 2005.

Address correspondence to:
Misako Nakashima, Ph.D.
Department of Oral Disease Research
National Center for Geriatrics and Gerontology
Research Institute
35 Gengo, Morioka, Obu
Aichi 474-8522
Japan

E-mail: misako@ncgg.go.jp

Received: May 24, 2010
Accepted: January 10, 2011
Online Publication Date: February 22, 2011

THE JOURNAL OF BIOLOGICAL CHEMISTRY VOL. 286, NO. 11, pp. 8952–8960, March 18, 2011

Plasminogen/Plasmin Modulates Bone Metabolism by Regulating the Osteoblast and Osteoclast Function*

Received for publication, June 7, 2010, and in revised form, January 4, 2011 Published, JBC Papers in Press, January 14, 2011, DOI 10.1074/jbc.M110.152181

Yosuke Kanno[‡1], Akira Ishisaki[§], Eri Kawashita[‡], Naoyuki Chosa[§], Keiichi Nakajima[¶], Tatsuji Nishihara[‖], Kuniaki Toyoshima[**], Kiyotaka Okada[‡‡], Shigeru Ueshima[‡‡§§], Kenji Matsushita[¶¶], Osamu Matsuo[‡‡], and Hiroyuki Matsuno[‡]

From the [‡]Department of Clinical Pathological Biochemistry, Faculty of Pharmaceutical Science, Doshisha Women's Collage of Liberal Arts, 97-1 Kodo Kyo-tanabe, Kyoto 610-0395, the [§]Department of Biochemistry, Iwate Medical University School of Dentistry, 1-3-27, Chuo-dori, Morioka, Iwate 020-8505, the [¶]Department of Animal Production and Grassland, National Agricultural Research Center for Hokkaido Region, 062-8555 Sapporo, the [‖]Division of Infections and Molecular Biology, Department of Health Promotion, Kyushu Dental College, 2-6-1 Manazuru, Kokurakita-ku, Kitakyushu 803-8580, the [**]Division of Oral Histology and Neurobiology, Department of Biosciences, Kyushu Dental College, 2-6-1 Manazuru, Kokurakita-ku, Kitakyushu 803-8580, the [‡‡]Department of Physiology II, Kinki University School of Medicine 377-2 Ohnohigashi, Osaka-sayama-city 589-8511, the [§§]Department of Food Science and Nutrition, Kinki University School of Agriculture, Nara 631-8505, and the [¶¶]Laboratory of Oral Disease Research, National Institute for Longevity Sciences, National Center for Geriatrics and Gerontology, 36-3 Gengo, Morioka, Obu, Aichi 474-8522, Japan

The contribution of plasminogen (Plg)/plasmin, which have claimed to be the main fibrinolytic regulators in the bone metabolism, remains unclear. This study evaluated how the absence of Plg affects the function of osteoblast (OB) and osteoclast (OC). There was a larger population of pre-OCs in bone marrow-derived cells from the $Plg^{-/-}$ mice than the population of that from the WT mice. In addition, the absence of Plg suppressed the expression of osteoprotegerin in OBs. Moreover, an exogenous plasmin clearly induced the osteoprotegerin expression in $Plg^{-/-}$ OBs. The osteoclastogenesis of RAW264.7 mouse monocyte/macrophage lineage cells in co-culture with OBs from the $Plg^{-/-}$ mice was significantly accelerated in comparison with that in co-culture with OBs from the WT mice. Intriguingly, the accelerated OC differentiation of RAW264.7 cells co-cultured with $Plg^{-/-}$ OBs was clearly suppressed by the treatment of an exogenous plasmin. Consequently, $Plg^{-/-}$ mice display decreased bone mineral density. These findings could eventually lead to the development of new clinical therapies for bone disease caused by a disorder of the fibrinolytic system.

The fibrinolytic system contains plasminogen (Plg),[2] a proenzyme, which is converted to the active serine protease plasmin, a main component of the fibrinolytic system, through the action of a tissue-type plasminogen activator (tPA) or urokinase-type PA (uPA). The inhibition of the system may occur through the neutralization of the plasminogen activators or plasmin, and this neutralization is achieved mainly by the plasminogen activator inhibitor-1 (PAI-1) or α2-antiplasmin (α2AP), respectively. PAI-1, the primary endogenous inhibitor of tPA or uPA, plays an important role in inhibiting arterial clot lysis (1). α2AP rapidly inactivates plasmin, resulting in the formation of a stable inactive complex, plasmin-α2AP (2). Apart from the removal of fibrin, the fibrinolytic system also plays a pivotal role in such phenomena as embryogenesis, proliferation, migration, wound healing, fibrosis, and tumorigenesis (3–9).

It is suggested that fibrinolytic factors such as tPA, uPA, uPA receptor, and PAI-1 are involved in bone metabolism as follows. The absence of tPA and uPA enhanced OB differentiation and formation of a mineralized bone matrix and increased bone formation and bone mass (10). The absence of PAI-1 protects against trabecular bone loss induced by estrogen deficiency, suggesting a site-specific role for PAI-1 in bone turnover (11). In addition, uPA receptor-lacking mice displayed increased bone mineral density (BMD), increased osteogenic potential of OBs, decreased OC formation, and cytoskeletal reorganization in mature OCs (12). However, the physiological roles of fibrinolytic main regulators such as Plg/plasmin in bone metabolism are not precisely understood.

The receptor activator of NF-κB (RANK), its ligand RANKL, and OPG control OC function (13, 14). RANK activated by RANKL has proven to be absolutely required for OC development (15). RANKL is neutralized by OPG that specifically binds to RANKL. OPG is expressed in many tissues apart from OBs, including heart, kidney, liver, spleen, and bone marrow (13). However, molecular mechanisms of OPG expression remain to be elucidated. We herein report the crucial role of fibrinolytic main regulators Plg/plasmin in bone metabolism especially on the point of view of how the regulators affect the ability of pre-OCs in bone marrow to differentiate into OCs, OBs to induce OC differentiation, and OBs to mineralize extracellular matrix.

* This work was supported by Grant-in-aid for Young Scientists B:21790097 (to Y. K.) from the Ministry of Education, Culture, Sports, Science and Technology, Japan Society for the Promotion of Science, and Grant-in-aid for Strategic Medical Science Research Center from the Ministry of Education, Culture, Sports, Science and Technology of Japan, 2010-2014.

[1] To whom correspondence should be addressed. Tel.: 81-0774-65-8629; Fax: 81-0774-65-8479; E-mail: ykanno@dwc.doshisha.ac.jp.

[2] The abbreviations used are: Plg, plasminogen; TRAP, tartrate-resistant acid phosphatase; OC, osteoclast; OB, osteoblast; OPG, osteoprotegerin; BMD, bone mineral density; PGE_2, prostaglandin E_2; RANK, receptor activator of NF-κB; RANKL, RANK ligand; tPA, tissue-type plasminogen activator; uPA, urokinase-type PA; PAI-1, plasminogen activator inhibitor-1; M-CSF, macrophage colony-stimulating factor; ALP, alkaline phosphatase; qRT, quantitative RT.

MATERIALS AND METHODS

All experiments were performed in accordance with the Guide for the Care and Use of Laboratory Animals published by the National Institutes of Health.

Animals—The Plg-deficient ($Plg^{-/-}$) mice (16) were kindly provided by Prof. D. Collen (University of Leuven, Belgium).

Wild type (WT) and $Plg^{-/-}$ mice littermates were housed in groups of two to five in filter-top cages with a fixed 12-h light, 12-h dark cycle. The body weights of mice were measured weekly.

Reagents—Plasmin, aprotinin, α2AP, ε-aminocaproic acid, and other chemical substances were obtained from Sigma.

Cell Culture—Bone marrow cells, RAW264.7 mouse monocyte/macrophage lineage cells (American Type Culture Collection), and primary OBs were maintained in α-minimal essential medium (Invitrogen) supplemented with 10% fetal bovine serum (FBS) (Hyclone, Logan, UT) and 1% penicillin/streptomycin (Invitrogen) at 37 °C in a humidified atmosphere of 5% CO_2, 95% air. Primary OBs derived from mice calvaria were obtained as described previously (17).

OC Differentiation Assay—Bone marrow-derived cells that include a population of pre-OCs were obtained from tibia of 5–7-week-old adult mice. Mouse bone marrow cells were cultured for 3 days with RANKL (100 ng/ml) and M-CSF (100 ng/ml) in 48-well plates. In other experiments, RAW264.7 cells were co-cultured with OBs from the $Plg^{+/+}$ and $Plg^{-/-}$ mice for 3 days in the absence or presence of interleukin-1β (IL-1β) (5 ng/ml) or prostaglandin E_2 (PGE_2) (1 μM) in 48-well plates. Cells were then fixed and stained for tartrate-resistant acid phosphatase (TRAP; a marker enzyme of OCs) as described previously (17). TRAP-positive multinucleated cells containing three or more nuclei were counted as OCs, under microscopic examination.

Bone Resorption Assay—To estimate bone resorption activity of differentiated OCs from bone marrow cells of the $Plg^{+/+}$ and $Plg^{-/-}$ mice, the cells were stimulated with RANKL (100 ng/ml) and M-CSF (100 ng/ml) for 7 days on the BioCoat™ Osteologic™ multiple test slides, which consisted of submicron synthetic calcium phosphate thin film coated onto various culture vessels (BD Biosciences). The nonresorbed area of calcium phosphate film was then visualized by using a method of von Kossa staining, as follows. After fixation of the cells in the culture with 5% glutaraldehyde, the calcium phosphate film was treated with 5% silver nitrate for 30 min. Then the staining was developed with 5% sodium carbonate in 25% formalin. The stained film in each well was photographed under light microscopy, and then the image was inverted to yield the negative image; the black image represents the resorbed area in the calcium phosphate film.

Bone Histology—Bone histomorphometry of tibia in 5-week-old male $Plg^{+/+}$ and $Plg^{-/-}$ mice was performed. Each tibia was removed and fixed in 4% paraformaldehyde for 2 days and then demineralized with 10% EDTA for 14 days before embedding in paraffin. Paraffin-embedded tissue was serially sectioned at a distance of 4–7 μm. Then the sections were stained with hematoxylin and eosin (H&E) and TRAP by using a TRAP kit (Sigma). For the quantitative evaluation of the intensity of TRAP staining of bone marrow tissue in decalcified sections of tibia from the $Plg^{+/+}$ and $Plg^{-/-}$ mice, the TRAP-stained images obtained from separate fields on the specimens ($n = 6$) were analyzed by using ImageJ.

Measurement of Bone Mineral Density—BMD was measured as described by Kanazawa *et al.* (18) and Nishiwaki *et al.* (19). BMD of the proximal tibia of the $Plg^{+/+}$ and $Plg^{-/-}$ mice at the indicated time was evaluated by using peripheral quantitative computed tomography with a fixed x-ray fan beam of 50-μm spot size, at 1 mA and 50 kV (LaTheta LCT-100S; Aloka, Tokyo, Japan).

RNA Isolation and Quantitative RT-PCR—Total RNA was extracted as described previously (6). First strand cDNA was synthesized from total RNA by using the PrimeScript RT reagent kit (Takara). Quantitative RT-PCR (qRT-PCR) was performed on the IQ5 real time PCR detection system (Bio-Rad) with SYBR Green technology on cDNA generated from the reverse transcription of purified RNA. The two-step PCRs were performed at 92 °C for 1 s and 60 °C for 10 s. OPG mRNA expression was normalized against GAPDH mRNA expression using the comparative cycle threshold method. We used the following primer sequence: OPG, 5′-CAATGGCTGGCTTGGTTTCATAG-3′ and 5′-CTGAACCAGACATGACAGCTGGA-3′; GAPDH, 5′-TGTGTCCGTCGTGGATCTGA-3′ and 5′-TTGCTGTTGAAGTCGCAGGAG-3′.

Western Blot Analysis—We performed a Western blot analysis for detection of OPG, phospho-ERK1/2, phospho-p38 MAPK, ERK1/2, and p38 MAPK as described previously (20). We detected OPG, phospho-ERK1/2, phospho-p38 MAPK, ERK1/2, and p38 MAPK by incubation with a polyclonal OPG antibody (rabbit IgG, from GeneTex Inc.), anti-phospho-ERK1/2 antibody (Cell Signaling Technology, Danvers, MA), anti-phospho-p38 MAPK antibody (Cell Signaling Technology, Danvers, MA), anti-ERK1/2 antibody (Cell Signaling Technology, Danvers, MA), and anti-p38 MAPK antibody (Cell Signaling Technology, Danvers, MA).

Measurement of Alkaline Phosphatase Activity—We measured alkaline phosphatase (ALP) activity as described previously (20). Primarily cultured OBs were cultured for 14 day with differentiation media (media supplemented with 10 mM β-glycerophosphate and 10 nM dexamethasone and 50 μg/ml ascorbic acid) in 6-well plates. After 14 days, cells were then washed, and proteins in cells were extracted with a lysis buffer (10 mM Tris-HCl, pH 7.5, 0.1% Triton X-100). ALP activity was determined using *p*-nitrophenyl phosphate (Sigma) as a substrate.

Statistical Analysis—All data are expressed as mean ± S.E. The significance of the effect of each treatment ($p < 0.05$) was determined by analysis of variance followed by the Student's Newman-Keuls test.

RESULTS

Histological and Radiological Evaluation of the Status of Endochondral Ossification in Plg-deficient Mice—The BMDs in the $Plg^{+/+}$ and $Plg^{-/-}$ mice at 4–20 weeks were radiologically assessed using peripheral quantitative computed tomography. Intriguingly, the trabecular BMD in tibia from the $Plg^{-/-}$ mice was significantly lower than that from the $Plg^{+/+}$ mice at 4–6 weeks after birth (Fig. 1*A*). In addition, the cortical BMD in tibia

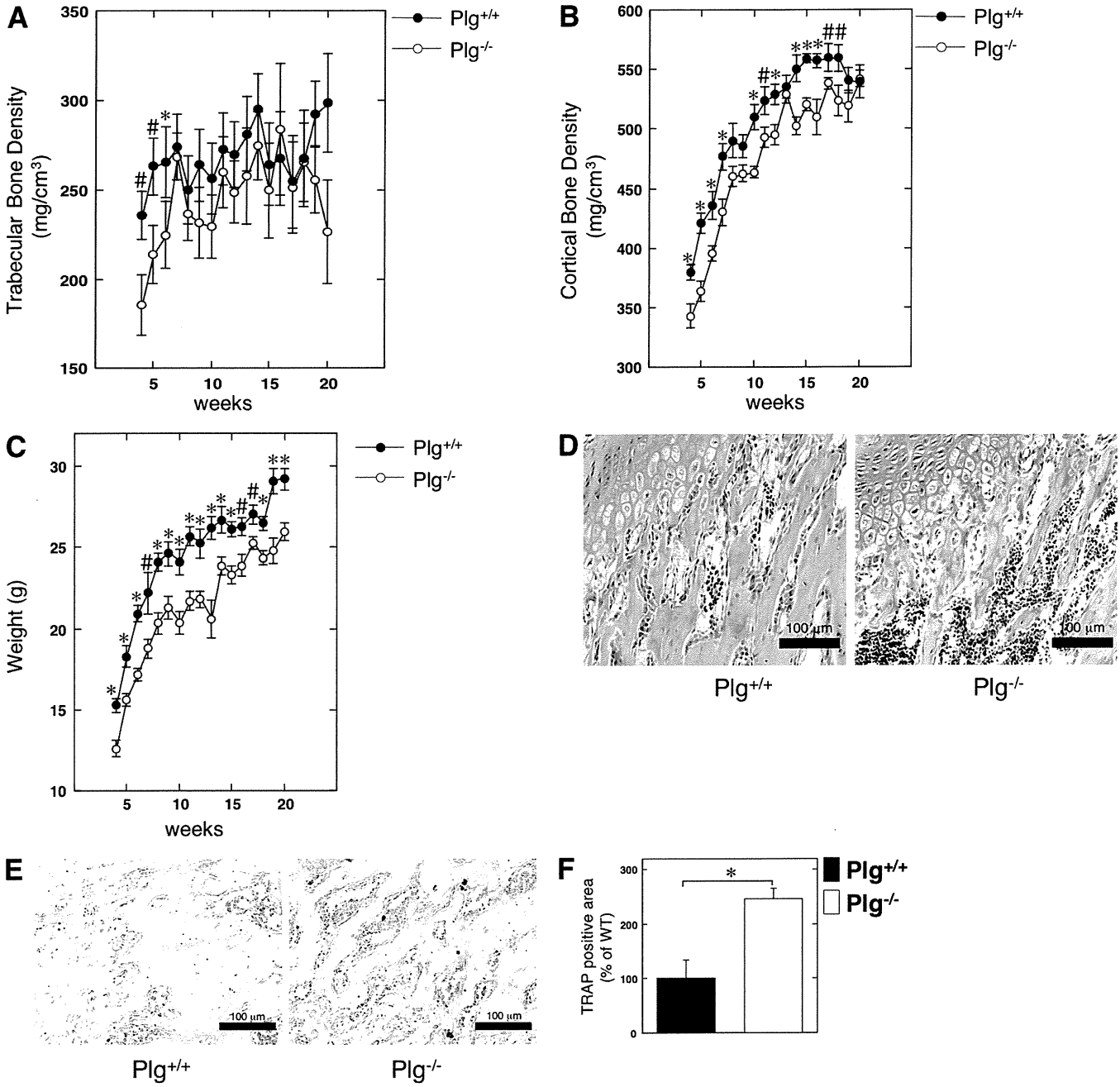

FIGURE 1. **Bone histomorphometry and bone mineral density in Plg-deficient mice.** *A*, trabecular BMD in the proximal tibia of male $Plg^{+/+}$ and $Plg^{-/-}$ mice was obtained from pQCT measurement ($n = 13$). *B*, cortical BMD in the proximal tibia of the $Plg^{+/+}$ and $Plg^{-/-}$ mice was obtained from pQCT measurement ($n = 13$). *C*, growth curves of the $Plg^{+/+}$ and $Plg^{-/-}$ mice ($n = 13$). *D* and *E*, bone histomorphometry of tibia in 5-week-old male $Plg^{+/+}$ and $Plg^{-/-}$ mice (*D*, H&E; *E*, TRAP). *D*, layer of chondrocytes and trabecular bone formation in the medullary cavities were observed in both $Plg^{+/+}$ and $Plg^{-/-}$ mice. *E*, TRAP-positive area in the bone marrow tissue of the tibias from $Plg^{-/-}$ mice was much larger than that in the tissue specimens obtained from $Plg^{+/+}$ mice. *F*, intensity of TRAP staining on the decalcified sections of bone marrow tissue in the $Plg^{+/+}$ and $Plg^{-/-}$ mice was quantitatively evaluated as described under "Materials and Methods" ($n = 6$). The intensity of TRAP staining on the sections from the $Plg^{-/-}$ mice was much stronger than that of sections from $Plg^{+/+}$ mice. The data represent the mean ± S.E. *, $p < 0.01$; #, $p < 0.05$.

from the $Plg^{-/-}$ mice was significantly lower than that from the $Plg^{+/+}$ mice at 4–18 weeks after birth (Fig. 1*B*). The decrease of cortical BMD seemed to parallel that of the body weight decrease in the $Plg^{-/-}$ mice at 4–18 weeks after birth (Fig. 1, *B* and *C*). Next, the status of endochondral ossification in tibia from the $Plg^{+/+}$ and $Plg^{-/-}$ was histologically compared to clarify the effect of the fibrinolytic system in bone metabolism. As shown in Fig. 1*D*, H&E staining of a decalcified section of tibia from the 5-week-old mice showed that the layer of chondrocytes and trabecular bone formation in the medullary cavities were observed in both $Plg^{+/+}$ and $Plg^{-/-}$ mice. The TRAP staining of the decalcified section of the tibias from the 5-week-old mice revealed that the area of TRAP-positive bone marrow tissue in the tibias from the $Plg^{-/-}$ mice was significantly larger than that of the tissue from the $Plg^{+/+}$ mice (Fig. 1*E*). In addition, the intensity of the TRAP staining on the decalcified sec-

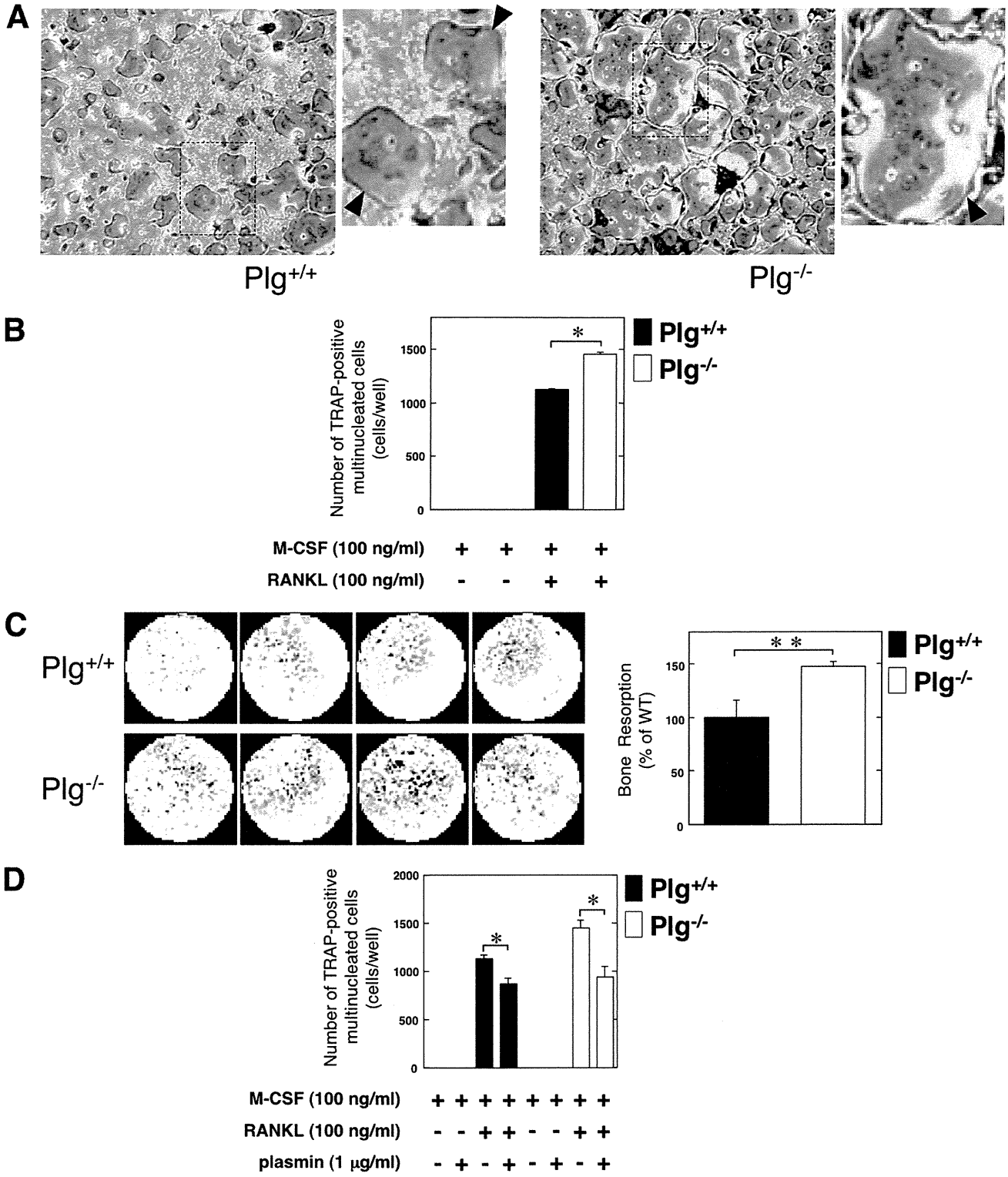

FIGURE 2. **Effect of Plg deficiency on osteoclastogenesis and the OC function.** *A*, bone marrow cells from the $Plg^{+/+}$ and $Plg^{-/-}$ mice were cultured for 3 days in the absence or presence of RANKL (100 ng/ml) and M-CSF (100 ng/ml). Mature OCs were identified as TRAP-positive multinucleated cells. The magnified image of *boxed area* was showed on the *right* of the original image. The *arrowheads* indicate osteoclasts. *B*, number of TRAP-positive multinucleated cells in *A* was determined from three different cultures. *C*, bone resorption activity of OCs differentiated from bone marrow-derived cells obtained from the $Plg^{+/+}$ and $Plg^{-/-}$ mice was compared. Bone marrow-derived cells from the $Plg^{+/+}$ and $Plg^{-/-}$ mice were cultured on the BioCoat™ Osteologic™ multiple test slides, which consisted of submicron synthetic calcium phosphate thin film coated onto various culture vessels, for 7 days in the presence of RANKL (100 ng/ml) and M-CSF (100 ng/ml) ($n = 4$). Next, the resorbed areas of the calcium phosphate film were visualized as described under "Materials and Methods." The *histogram, right panel*, shows quantitative representations of bone resorption obtained from densitometry analysis. The densitometry results were expressed as the mean density. *D*, bone marrow cells from the $Plg^{+/+}$ and $Plg^{-/-}$ mice were cultured for 3 days in the presence of M-CSF (100 ng/ml). Some cells were cultured in the presence or absence of RANKL (100 ng/ml) or plasmin (1 μg/ml) as indicated. The number of multinucleated TRAP-positive cells was determined from four different cultures. The data represent the mean ± S.E. *, $p < 0.01$; **, $p < 0.05$.

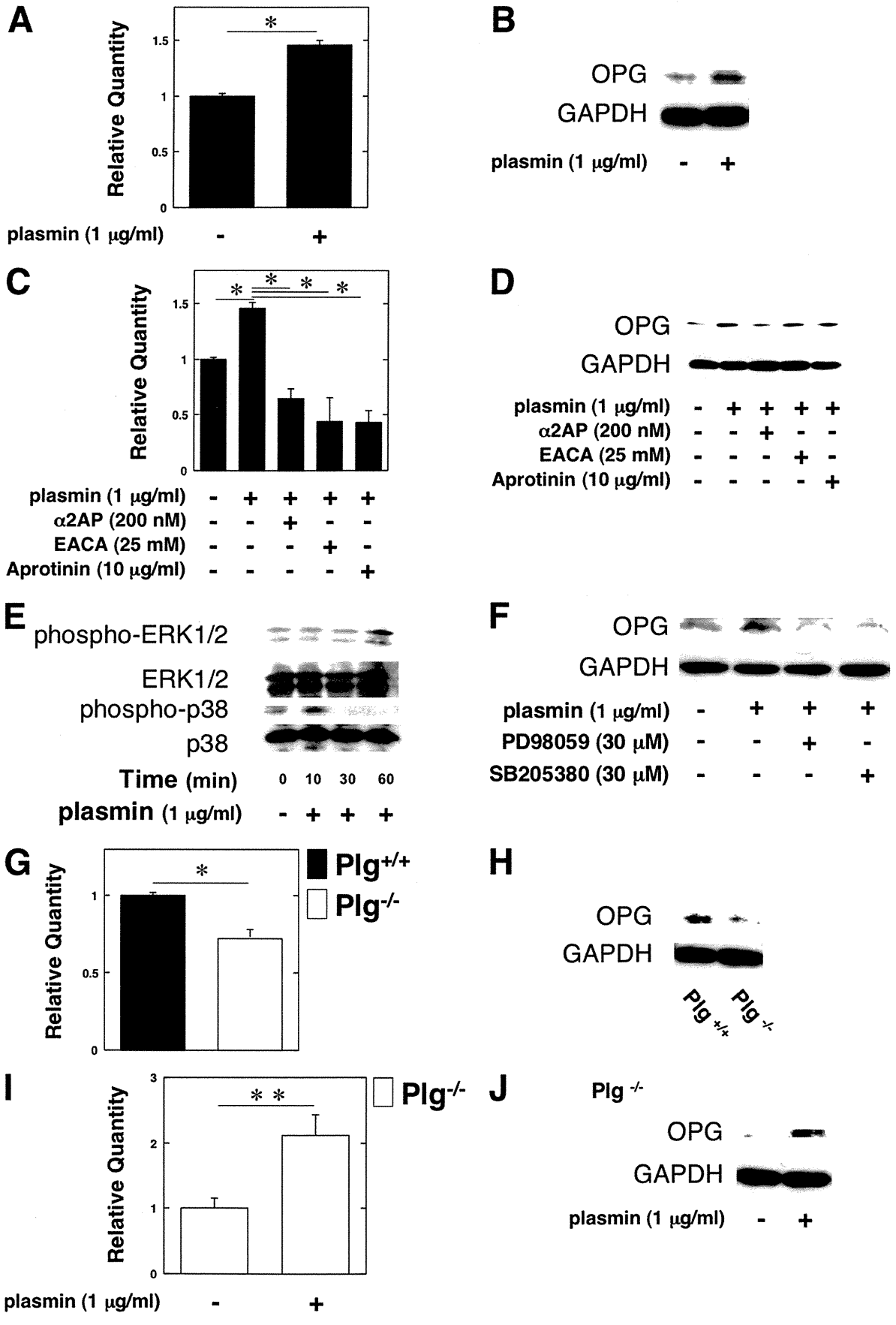

tions of bone marrow tissue in the $Plg^{+/+}$ and $Plg^{-/-}$ mice was quantitatively evaluated as described under "Materials and Methods." As shown in Fig. 1*F*, the intensity of TRAP staining on decalcified sections of bone marrow tissue in tibias from the $Plg^{-/-}$ mice was much stronger than in those from the $Plg^{+/+}$ mice.

Effect of the Plg Deficiency on the Osteoclastogenesis of Bone Marrow-derived Cells—We evaluated how the fibronolytic system affects OC differentiation and function. The pre-OC population in bone marrow-derived cells from the $Plg^{+/+}$ and $Plg^{-/-}$ mice were evaluated after stimulation with RANKL and M-CSF, respectively. As shown in Fig. 2*A*, many TRAP-positive multinucleated OCs were observed in bone marrow cell cultures derived from the $Plg^{-/-}$ mice tibia. Therefore, an up-regulation of the TRAP-positive cell number in the $Plg^{-/-}$ mice-derived bone marrow cells was observed (Fig. 2*B*). In addition, the bone resorption activity of OCs differentiated from bone marrow-derived cells was compared in the $Plg^{+/+}$ and $Plg^{-/-}$ mice. There was an up-regulation of the bone resorption activity of $Plg^{-/-}$ mice-derived bone marrow cells (Fig. 2*C*). Intriguingly, plasmin significantly inhibited the M-CSF- and RANKL-induced OC differentiation of bone marrow cells derived from the $Plg^{-/-}$ and $Plg^{+/+}$ mice (Fig. 2*D*).

Plasmin Induced the OPG Expression in OBs—To clarify how plasmin suppresses osteoclastogenesis *in vivo*, we examined whether plasmin up-regulates the expression of OPG in OBs from the WT mice *in vitro* by qRT-PCR and a Western blot analysis. Plasmin clearly induced OPG expression in OBs from the WT mice (Fig. 3, *A* and *B*). In addition, the effect of various plasmin inhibitors (α2AP; serine protease inhibitor, aprotinin; lysine analog, ϵ-aminocaproic acid) on plasmin-induced OPG expression was investigated. These plasmin inhibitors clearly abrogated the plasmin-induced OPG expression (Fig. 3, *C* and *D*).

In addition, we examined the plasmin-stimulated phosphorylation of ERK1/2 and p38 MAPK to determine whether plasmin activates ERK1/2 and p38 MAPK in OBs. Plasmin activated ERK1/2 and p38 MAPK in OBs (Fig. 3*E*). We also examined whether the ERK1/2 and p38 MAPK pathways are associated with the plasmin-induced expression of OPG in OBs by using the inhibitor of MEK and p38 MAPK (PD98059 and SB203580). PD98059 and SB203580 attenuated plasmin-induced expression of OPG in OBs (Fig. 3*F*). These data suggest that plasmin induces OPG expression through the ERK1/2 and p38 MAPK pathways.

Moreover, qRT-PCR and a Western blot analysis revealed that the expression of OPG was suppressed in OBs from the $Plg^{-/-}$ mice (Fig. 3, *G* and *H*), thus suggesting that the absence of plasmin may result in the acceleration of osteoclastogenesis of pre-OCs in accordance with the depletion of OPG synthesis in OBs. There was no difference in the status of RANKL mRNA expression in OBs from the $Plg^{+/+}$ and $Plg^{-/-}$ mice (data not shown). Moreover, plasmin induced OPG expression in $Plg^{-/-}$ OBs (Fig. 3, *I* and *J*).

Effects of Plg Deficiency on the Ability of OBs to Induce Osteoclastogenesis of RAW264.7 Mouse Monocyte/Macrophage Lineage Cells—The status of OC differentiation of RAW264.7 mouse monocyte/macrophage lineage cells in co-culture with $Plg^{-/-}$ OBs was examined to clarify how Plg deficiency affects OB function for osteoclastogenesis. The ability of $Plg^{-/-}$ OBs to induce OC differentiation of pre-OC RAW264.7 cells was compared with $Plg^{+/+}$ OBs. The OBs were co-cultured with RAW264.7 cells under stimulation with the inflammatory mediators interleukin 1-β (IL-1β) or prostaglandin E_2 (PGE_2). Inflammatory mediators induce RANKL expression on OBs (21). The inflammatory mediator-induced RANKL expression on OBs was expected to induce the osteoclastogenesis of the co-cultured RAW264.7 cells. As shown in Fig. 4*A*, IL-1β or PGE_2 increased the number of TRAP-positive multinucleated cells co-cultured with OBs. Intriguingly, the number of TRAP-positive multinucleated cells co-cultured with $Plg^{-/-}$ OBs lacking OPG expression was significantly higher than that co-cultured with $Plg^{+/+}$ OBs with or without IL-1β or PGE_2. In addition, the number of TRAP-positive multinucleated cells co-cultured with $Plg^{-/-}$ OBs was decreased by plasmin (Fig. 4*B*).

Effect of Plg Deficiency on the ALP Activity in OBs—The ALP activity in $Plg^{-/-}$ OBs was compared with $Plg^{+/+}$ OBs under stimulation with OB differentiation media as described under "Materials and Methods." The absence of Plg did not affect the ALP activity in undifferentiated and differentiated OBs (Fig. 5).

Rescue of the Down-regulated BMD in Plg-deficient Mice by the Injection of Plasmin—To clarify the effect of exogenous plasmin on bone formation *in vivo*, we evaluated the status of the BMD in the $Plg^{-/-}$ mice with or without plasmin injection. The plasmin injection clearly increased the trabecular BMD in the $Plg^{-/-}$ mice (Fig. 6*A*). However, the plasmin injection did not affect the cortical BMD and the weight in the $Plg^{-/-}$ mice (Fig. 6, *B* and *C*).

DISCUSSION

Fibrinolytic factors have been suggested to play an important role in bone metabolism. PAs and PAI-1 are involved in bone resorption by OCs (22, 23). However, the role of Plg/plasmin in bone metabolism was not precisely understood. This study showed that Plg/plasmin plays an important role in bone metabolism by regulating the function of both OBs and OCs.

FIGURE 3. **Plasmin induced the OPG expression in OBs.** *A–D*, OBs from the WT mice were cultured for 24 h in either the absence or presence of plasmin (1 μg/ml). Plasmin-induced expression of OPG gene in OBs from the WT mice was evaluated by qRT-PCR (*A*) or a Western blot analysis (*B*). *C* and *D*, some cultures were further treated with plasmin inhibitors as follows: α2AP (200 nM), ϵ-aminocaproic acid (25 mM), and aprotinin (10 μg/ml). The expression of OPG mRNA in OBs from the WT mice was then measured by qRT-PCR (*C*) or a Western blot analysis (*D*). *E*, OBs from the WT mice were stimulated with 1 μg/ml plasmin for the indicated periods. Phosphorylation of ERK1/2 and p38 MAPK was evaluated by a Western blot analysis using antibodies to ERK1/2 and p38 MAPK. *F*, OBs from the WT mice were pretreated with 30 μM PD98059 or 30 μM SB203580 for 60 min and then stimulated with 1 μg/ml plasmin for 24 h. The expression of OPG in OBs from the WT mice was evaluated by a Western blot analysis. *G* and *H*, OPG expression in OBs from the $Plg^{+/+}$ and $Plg^{-/-}$ mice was evaluated by qRT-PCR (*G*) or a Western blot analysis (*H*). *I* and *J*, OBs from the $Plg^{-/-}$ mice were cultured for 24 h in the absence or presence of plasmin (1 μg/ml). The OPG expression in OBs from the $Plg^{-/-}$ mice was evaluated by qRT-PCR (*I*) or a Western blot analysis (*J*). The data represent the mean of three individual experiments ± S.E. *, $p < 0.01$; **, $p < 0.05$.